Pergamon

Geochimica et Cosmochimica Acta, Vol. 58, No. 4, pp. 1313–1334, 1994

0016-7037/94 $6.00 + .00

Petrography, composition, and origin of large, chromian spinels from the Murchison meteorite

S. B. SIMON,[1] L. GROSSMAN,[1,2] F. A. PODOSEK,[3,4] E. ZINNER,[3,5] and C. A. PROMBO[3,4]

[1]Department of Geophysical Sciences, The University of Chicago, 5734 South Ellis Avenue, Chicago, IL 60637, USA
[2]Enrico Fermi Institute, The University of Chicago, 5630 South Ellis Avenue, Chicago, IL 60637, USA
[3]McDonnell Center for the Space Sciences, Washington University, One Brookings Drive, St. Louis, MO 63130-4899, USA
[4]Department of Earth and Planetary Sciences, Washington University, St. Louis, MO 63130, USA
[5]Department of Physics, Washington University, St. Louis, MO 63130, USA

(*Received March* 2, 1993; *accepted in revised form September* 24, 1993)

Abstract—Most spinel grains in Murchison acid residues are Mg-, Al-rich, ^{16}O-rich ($\delta^{18}O = -50‰$), small (10–30 μm) and probably from refractory inclusions. They are quite unlike spinels we have recovered from Murchison by freeze-thaw disaggregation, density separation, and handpicking. As reported here, the latter spinels contain up to 37 wt% Cr_2O_3 and up to 17 wt% FeO, are not ^{16}O-enriched ($\delta^{18}O = 1.9 \pm 2.4‰$), are coarse (60–325 μm), and are not from refractory inclusions. From backscattered electron images of fifty-seven such grains, we recognize five zoning types defined by variations in Cr_2O_3 contents: patchy (56%); homogeneous (21%); chevron (10.5%); gradational (9%); and core-rim (3.5%). Many grains have silicate inclusions, the most common being small, anhedral grains of diopside with 12–24 wt% Al_2O_3 and up to 3.7 wt% TiO_2. Eleven spinel samples occur with forsteritic (Fo_{95-99}) olivine; in most cases, the spinel partially encloses the olivine. Cr-bearing spinel was found in situ in two Al-rich chondrules (one with homogeneous spinel, the other with homogeneous, gradational and core-rim spinel, and both with forsterite and aluminous diopside); in two irregularly shaped, olivine-bearing inclusions (one with homogeneous spinel, the other patchy); and attached to an isolated olivine grain (patchy). Observation of homogeneous, gradational, and core-rim type spinels in chondrules and basalts shows that grains with these zoning patterns can crystallize from liquids, although, in Murchison, chondrules with the appropriate compositions and sufficiently coarse textures to yield the separated spinels are exceedingly rare. Chevron-zoned grains also could have formed in chondrules; alternatively, they may have acquired their oscillatory zoning patterns by cycling through different P-T-f_{O_2} regimes in the solar nebula during their formation. The patchy spinel grains were probably never molten and they most likely formed by sintering of aggregates of smaller spinel grains which were enriched in Cr and Fe to varying degrees. In spite of their various crystallization and thermal histories, the spinels all have normal oxygen and chromium isotopic compositions, consistent with formation from a single, well-mixed nebular reservoir. Based on the known slow rates of diffusion of oxygen in MgO, Al_2O_3, and $MgAl_2O_4$, it is unlikely that the spinels of this study formed from an isotopically anomalous reservoir and later re-equilibrated with a normal one; it is more likely that they have retained their original isotopic compositions. We see no evidence for anomalous Cr, which had been reported by others.

INTRODUCTION

SPINEL GRAINS FROM the Murchison (CM2) meteorite have been of interest ever since CLAYTON and MAYEDA (1984) reported large ^{16}O enrichments ($\delta^{18}O = -40‰$) in a bulk, spinel-rich aliquot of acid residue 2C10c. ZINNER and EPSTEIN (1986) found large ^{13}C excesses in spinel grains from Murchison acid residue CFOc and, at the time, could not rule out the possibility that the anomalous C was truly incorporated in the spinel. This led KUEHNER and GROSSMAN (1987) to study spinel grains recovered from Murchison by freeze-thaw disaggregation, heavy liquid (density) separation, and handpicking, with the goal of petrographically characterizing the spinels with isotopically anomalous carbon. Ion probe analysis of the grains described by KUEHNER and GROSSMAN (1987) showed, however, that they have isotopically normal carbon and oxygen (GROSSMAN et al., 1988). An additional, important difference between the handpicked spinel grains and those in the acid residues is that the former are coarse: 60–325 μm vs. 3–50 μm (but mostly 3–10 μm) in 2C10c and 10–30 μm in CFOc. Unlike CLAYTON and MAYEDA (1984), who analyzed a bulk separate, VIRAG et al. (1991) used an ion probe to measure oxygen isotopic compositions of individual grains of spinel recovered from Murchison acid residue CFOc. They found that grains of pure Mg-, Al-spinel had even greater ^{16}O enrichments ($\delta^{18}O = -50‰$) than the residue analyzed by CLAYTON and MAYEDA (1984). VIRAG et al. (1991) concluded that the Mg-rich spinel grains which they analyzed belong to an ^{16}O-rich population, the relatively Cr-rich (up to 37 wt% Cr_2O_3 vs. <5900 ppm in the CFOc grains) spinel analyzed by GROSSMAN et al. (1988) represent an ^{16}O-poor group, and the spinel analyzed by CLAYTON and MAYEDA (1984) is a mixture of the two.

Chromium isotopic analyses may also indicate that there are two types of spinel in Murchison. Spinels in common refractory inclusions are characterized by modest but well-established and endemic ^{54}Cr excesses of 5–10 ϵ-units (parts in 10^4) and ^{53}Cr deficits of 1–2 ϵ-units, relative to assumed normal ^{50}Cr/^{52}Cr (PAPANASTASSIOU, 1986; BIRCK and ALLÈGRE, 1988). In contrast, ESAT and IRELAND (1989) reported much larger (several permil) and variable chromium

isotopic anomalies in Murchison spinels of the type considered here, which would suggest that these spinels formed from a much narrower class of presolar materials than the spinels from refractory inclusions.

The ^{16}O-rich, Mg-, Al-spinels are probably from refractory inclusions (MACPHERSON et al., 1983, 1984a; IRELAND et al., 1992), but little is known about the origin of the ^{16}O-poor, Cr-bearing spinels. These grains are the subject of the present study, in which we use detailed petrographic, mineral-chemical, and isotopic (O and Cr) data to constrain their origins and histories. Some preliminary results of this study were reported by KUEHNER and GROSSMAN (1987), GROSSMAN et al. (1988), PODOSEK et al. (1991), and SIMON and GROSSMAN (1992). Also, MACPHERSON et al. (1983) studied samples SP2-SP7, which are included in the present suite of samples.

ANALYTICAL TECHNIQUES

Sample Preparation, Scanning Electron Microscopy, and Electron Probe Microanalysis

Chips of Murchison were disaggregated using the freeze-thaw method described by MACPHERSON et al. (1980). Spinel grains were handpicked from the densest fraction ($\rho > 3.50$), examined with a binocular microscope, and identified on the basis of color (pink, red, or purple), high refractive index and, where possible, octahedral shape (KUEHNER and GROSSMAN, 1987). Some grains were split, with separate chips used for ion microprobe and thermal ionization mass spectrometric analysis and another mounted in epoxy for petrographic study. Other grains (SP51-SP81) were not split and were only mounted in epoxy. Six grains (SP22, SP25, SP26, SP32, SP34, and SP35) were either plucked or not sufficiently polished for petrographic study. Polished sections of all remaining fifty-seven grains were examined with a JEOL JSM-35 scanning electron microscope (SEM) operated at 10 kV and 2–3 nA. This relatively high current was used to obtain increased contrast in backscattered electron images (BEI), revealing smaller composition variations within spinel grains than can be observed at normal operating currents. Wavelength-dispersive analyses of spinel and attached phases were performed with a fully automated Cameca SX-50 electron microprobe. Synthetic glass and crystal (spinel, thortveitite, rutile, Cr_2O_3) and natural mineral (P-140 olivine, andradite) standards were used. Except for the analyses plotted in Fig. 5, which were all collected at 15 kV and 40 nA, data for major elements were collected at 15 kV with a beam current of 25 nA, and for minor elements (e.g., Ti and V in spinel and olivine) at 25 kV and 200 nA. This was done with an automated routine in which each point was analyzed for major elements, then the accelerating voltage and beam current settings needed for minor element analysis were loaded automatically, and the same point was analyzed for trace elements without moving the stage. Background count rates were measured at offsets below and above each peak position for a total counting time equal to that used for the peak. Data were reduced via the modified ZAF correction procedure PAP (POUCHOU and PICHOIR, 1984).

Ion Microprobe Analysis

For the oxygen isotopic measurements, fragments of spinel crystals were pressed into gold foil along with Burma spinel (USNM#135273), a terrestrial standard whose isotopic composition had previously been determined to be $\delta^{17}O_{SMOW} = +11.6‰$ and $\delta^{18}O_{SMOW} = +22.1‰$ by conventional gas mass spectrometry (R. N. CLAYTON and T. K. MAYEDA, pers. commun.). The technique for oxygen isotopic analysis with the Washington University ion microprobe, a modified CAMECA IMS 3F, has previously been described by MCKEEGAN (1987), FAHEY et al. (1987), and VIRAG et al. (1991). Oxygen was detected as negative secondary ions produced by Cs^+ bombardment. A mass resolving power of 6500 was sufficient to resolve $^{17}O^-$ from $^{16}OH^-$. Measurements on Murchison spinel samples were interspersed with measurements on the terrestrial standard. The meteoritic data were normalized by comparing the average of the Burma spinel data to the known composition of this standard.

Thermal Ionization Mass Spectrometry

Splits of some of the same grains that were analyzed for oxygen isotopes were also analyzed for chromium isotopes. For chromium isotopic analysis we used a "direct-load" procedure in which spinel grain fragments were loaded with silica gel and boric acid onto V-shaped Re mass spectrometer filaments. Isotopic analyses were performed in the Washington University VG-354 thermal ionization mass spectrometer; all measurements were made with a Daly detector operated in pulse-counting mode. As calibrations for Cr, we used the same Burma spinel employed for calibration of the ion probe oxygen analyses and also a reagent Cr solution, both loaded the same way as the Murchison spinels. All data were acquired with a beam intensity of $\sim 2 \times 10^5$ cps of ^{52}Cr. Ion isotopic ratios were corrected for instrumental discrimination assuming terrestrial normal $^{50}Cr/^{52}Cr$ as reported by SHIELDS et al. (1966) and the "exponential" mass dependence described by RUSSELL et al. (1978). Results for ^{53}Cr and ^{54}Cr abundances are reported as ϵ-unit deviations from the terrestrial normal composition reported by PAPANASTASSIOU (1986).

Potential isobaric interferences from ^{50}Ti and ^{54}Fe were monitored at masses 49 and 56 amu, respectively, with formal corrections made assuming normal titanium and iron isotopic compositions. In practice, no Ti signal above a few counts per second was identifiably detected in any of these analyses, and the formal corrections based on mass 49 are trivial ($\leq 0.2\epsilon$). An Fe ion signal, monitored at mass 56, was generally found to be present. In some analyses, the corresponding correction to ^{54}Cr was substantial (several hundred ϵ). Even in such cases the *corrected* $^{54}Cr/^{52}Cr$ agreed as well as could be determined (i.e., within several ϵ) with data acquired for the same sample during other parts of the analysis when the Fe interference was much lower, which gives us confidence that the 56 signal is correctly identified as Fe. The data reported do not include any analyses involving an Fe correction greater than 10ϵ and, for most of these data, the correction is substantially smaller (no more than a few ϵ and in many cases $<1\epsilon$). We consider the *uncertainty* in the Fe correction not to be a significant contribution to overall uncertainty.

Data acquisition and reduction were organized into "sets," where each set comprises five cycles through the chromium isotopes, integrating for five seconds at each field setting, plus baseline and interference measurements. Beam intensity regulation, ion source focusing, magnetic field adjustments, and various diagnostics were performed between sets. A "run" is a collection of sets, up to a maximum of 100 sets, for which the isotope ratios of interest ($^{50}Cr/^{52}Cr$, $^{53}Cr/^{52}Cr$, and $^{54}Cr/^{52}Cr$) are taken as the means of the ratios calculated for each set, with uncertainties ("internal" errors) based on the variances of the set ratios about their mean. Under ideal circumstances, when no other sources of error are important, precision in isotopic ratio measurement is limited by Poisson statistics for the number of ions detected. For the protocol described above, the one-sigma Poisson limits for one set, including the errors in the ^{52}Cr and ^{50}Cr measurements, are 18ϵ for ^{53}Cr and 34ϵ for ^{54}Cr. Set-to-set variations agree well with Poisson statistics, indicating no sources of error that are significant compared to internal statistics and that operate on a set-to-set timescale.

The samples studied here were generally run to exhaustion, i.e., until they could no longer produce a satisfactory ion beam. This generally involved multiple runs, including repeat runs on the same filament load and more than one filament load for the same sample. The data reported in this paper, including those for reagent Cr and Burma spinel, are weighted means, and errors of the means, for all runs on a given sample. In aggregate, the data for Burma spinel are normal within formal errors, but the data for reagent Cr are not (Table 8). We take this as evidence for the presence of some source(s) of analytical error at a level which is not prominent compared to statistical errors for a single run but which becomes prominent when the statistical errors are formally reduced by convergence of the mean for a large number of runs (thirty-one runs for reagent Cr). The nature of such sources of error is unknown; one possibility is second-order mass dependence of instrumental discrimination, which might

be especially relevant in comparing reagent on the one hand with direct-loaded solid crystals on the other. Probably the best estimate for systematic errors in this procedure for Cr analysis is provided by the degree to which the reagent Cr deviates from assumed normal, i.e., around 2ϵ for ^{53}Cr and 5ϵ for ^{54}Cr, less than single-run statistical errors and much less than the size of the effects we wish to study here.

SAMPLE DESCRIPTIONS

Zoning Patterns in Spinel

When viewed with the binocular microscope, each spinel grain is translucent, uniform in color and luster, and completely homogeneous from one edge to the other. Some of these spinel grains are bounded by crystal faces, but not on all sides. When viewed at higher magnification with the petrographic microscope and SEM, the interiors of most samples are seen to contain few cracks or cavities whose presence would indicate polycrystallinity. Although the isotropism of spinel prevents optical confirmation, there is no indication that these grains are anything but single crystals, although some have attached grains and/or inclusions of phases other than spinel. There are perhaps four samples with inclusion or cavity patterns which suggest that those samples may consist of many small grains rather than one large crystal.

In backscattered electron images (BEIs), brightness correlates directly with the average atomic number of the sample, which, in the case of the spinel grains being considered here, depends mainly on the Cr_2O_3 (and, in some cases, FeO) contents of the spinel. High-contrast BEIs of these samples can reveal composition differences as small as $\sim$2 wt% Cr_2O_3. From examination of BEIs of each grain, we have recognized five different zoning patterns with respect to spatial variation of Cr_2O_3 contents. In addition, in most grains, increases in Cr_2O_3 are accompanied by increases in Ti (reported as TiO_2) and V_2O_3, but there is no systematic correlation with Mg/Fe. Petrographic and chemical features of each grain are summarized in Table 1. In order of decreasing abundance, the zoning types are patchy (56%), homogeneous (21%), chevron (10.5%), gradational (9%), and core-rim (3.5%). Each type is described below.

Patchy

Four examples of this type are shown in Fig. 1a–d, and they illustrate some of the differences among grains of this type. Patchy grains are characterized by numerous islands, typically 10–20 μm (but up to 100 μm) across, of contrasting Cr_2O_3 contents. In some grains, such as SP41 (Fig. 1a), the patches are rounded and irregularly shaped. In others, such as SP60 (Fig. 1b), the patches have relatively straight boundaries and are square to rectangular. Some have patches with sharp boundaries (SP41) and others, like SP51 (Fig. 1c), do not. Some have patches evenly distributed throughout the grain, whereas in others, such as SP64 (Fig. 1d), the patches are concentrated in one part of the grain. Aluminous diopside inclusions, commonly associated with voids, are present in many of the patchy spinels and are discussed in a later section. Although there are aureoles (typically Cr-poor) around the inclusions in a few grains, neither the inclusions nor the voids appear to be related, in general, to the distribution of patches within their host grains.

Table 1. Summary of characteristics of separated spinel grains.

Sample No.	Cr_2O_3 (range, wt %)	FeO (range, wt %)	<----------Inclusions----------> Al-Diop	Olivine	Glass	Other
Patchy						
SP2	23-25	8	X	---	---	---
SP4	7.3-13.7	0.5	X	X	---	NiFe
SP6	3.5-5.2	0.3	X	X	---	---
SP7	12.0-16.5	14	X	---	---	Ca-, Fe-sil
SP23	1.7-5.4	1.0	X	X	---	---
SP24	6.0-8.5	0.6	---	---	---	---
SP30	0.6-3.0	0.5	X	---	---	Fe-sil
SP31	9.0-18.0	4.0-7.0	---	---	---	Fe-sil
SP41	2.5-10.0	0.5	X	---	---	---
SP43	16.0-23.0	6.7	---	---	---	---
SP46	2.6-6.2	0.3	---	---	---	---
SP51	0.8-8.4	0.7	X	---	---	---
SP53	14.0-21.6	1.0	X	---	---	NiFe
SP54	10.5-12.0	1.5	---	---	X	---
SP55	6.5-14.5	1.0	X	---	---	---
SP56	7.9-10.7	2.0	X	---	---	NiFe
SP58	3.7-11.2	1.0	X	---	---	Fe-sil
SP60	9.5-12.1	0.7	X	---	---	NiFe
SP63	16.1-18.8	3.6	---	---	X	---
SP64	4.6-12.3	2.7-4.2	X	---	X	---
SP66	5.2-9.5	0.8	X	---	---	An
SP69	11.5-16.3	4.7	---	---	X	---
SP70	19.2-24.2	5.0	X	X	---	Fe-sil
SP71	6.7-12.1	0.9	X	X	---	Fe-sil
SP72	14.9-27.8	1.6-2.1	---	X	---	Fe-sil
SP74	19.6-22.3	4.3-5.5	X	---	---	Fe-sil
SP75	20.6-23.0	4.9	X	---	---	Fe-sil
SP77	3.9-6.3	0.6	---	---	---	Fe-sil
SP78	20.1-22.5	4.4-4.9	---	---	---	Fe-sil
SP79	20.6-23.7	4.8-5.3	X	X	---	Fe-sil, En
SP80	25.8-28.8	8.5	---	---	---	---
SP81	7.3-11.6	2.9	X	---	---	Ca-sil
Homogeneous						
SP21	6.0-7.0	0.8	---	---	---	---
SP29	8-10	1.5	---	---	---	---
SP33	3	0.25	---	---	---	---
SP36	1.5-2.0	0.5	---	---	---	---
SP47	14.5-15.7	5.5	---	---	---	---
SP52	35.7-36.9	16.0-17.0	---	---	---	---
SP57	22.0-23.6	6.7	---	---	---	---
SP59	2.6	0.1	---	---	---	NiFe
SP61	16.0-16.4	6.0	---	X	---	NiFe
SP65	15.4-15.6	5.7	---	---	---	---
SP68	2.7-3.0	0.2	---	---	---	Fe-sil
SP73	3.7-4.3	0.5	---	X	---	Fe-sil
Gradational						
SP3	14.5-24.2	6.0-7.0	---	---	---	---
SP27	6.1-14.3	2.5-6.0	---	---	---	Ca-sil
SP42	4.0-5.9	1.0	---	---	---	---
SP45	2.2-4.3	0.2	---	---	---	---
SP48	18-20	5.5-6.0	---	---	---	Fe-sil
Chevron						
SP44	0.3-6.0	0.8	X	---	X	---
SP49	16.2-20.2	6.4-7.8	---	---	---	---
SP50	15.4-21.2	6.0	X	X	---	NiFe
SP62	3.0-7.8	0.7	X	X	---	FeS
SP67	2.0-15.0	3.4-4.4	---	---	---	---
SP76	1.3-4.7	0.2-0.5	---	---	---	Fe-sil
Core-rim						
SP5	1.2-5.5	0.65	X	---	---	NiFe
SP28	1.0-7.0	0.7	X	---	---	---

Ranges determined by energy dispersive analysis have fewer significant figures than those determined by wavelength dispersive analysis.
An "X" indicates that the phase is present. Al-diop: aluminous diopside; En: enstatite; An: anorthite; Fe-sil: Fe-silicate; Ca-sil: Ca-silicate.

Homogeneous

Twelve of the fifty-seven grains we studied appear homogeneous, with internal ranges in Cr_2O_3 contents $\leq$ 2 wt% and no discernible electron albedo differences in high-contrast BEI. These grains typically have no inclusions.

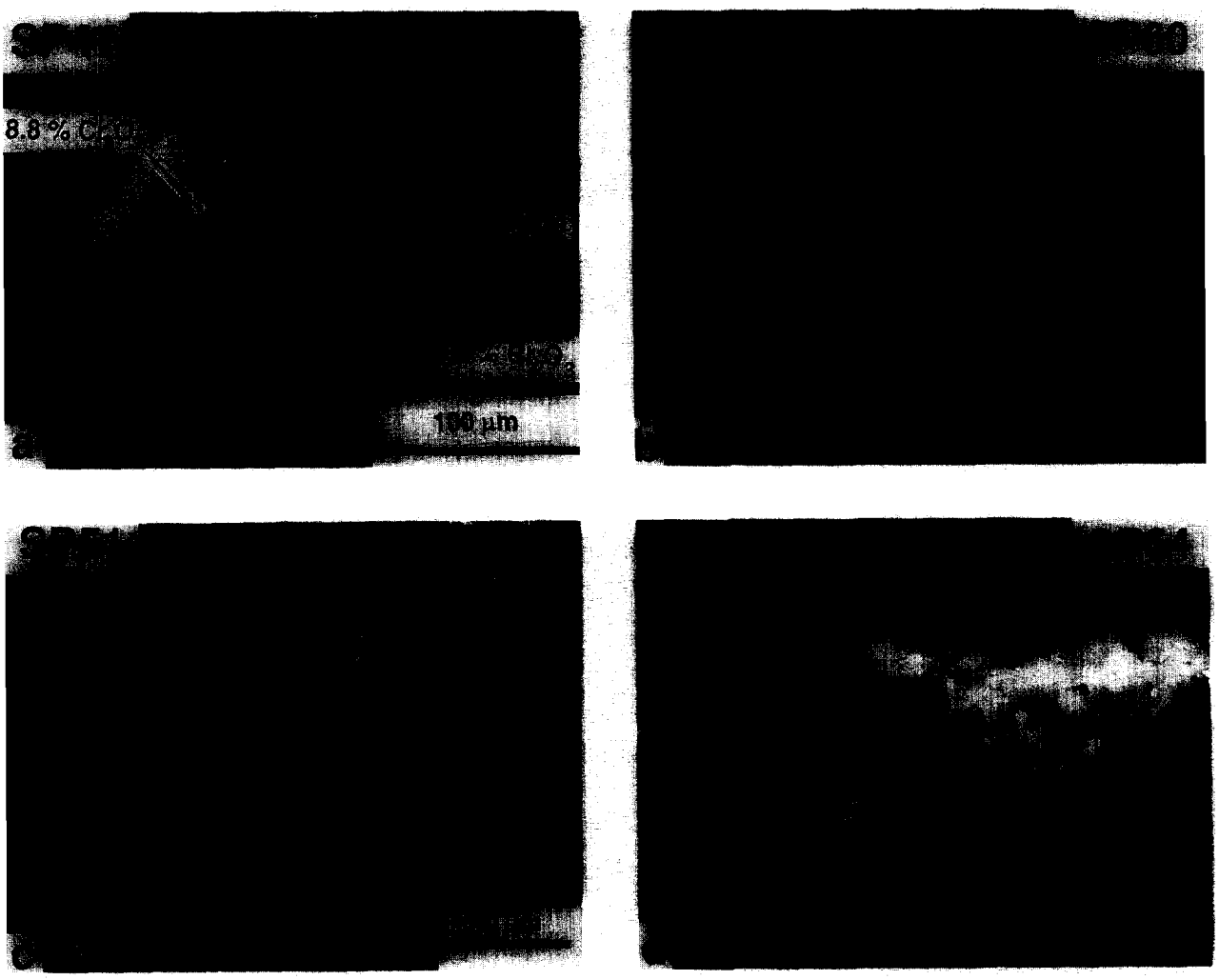

FIG. 1. Backscattered electron images (BEI) of spinel grains which represent the various zoning types. Lighter regions within spinel are zones of relatively high Cr_2O_3 content. (a) Patchy spinel. Very bright grains within the spinel are inclusions of aluminous diopside. (b) Patchy spinel, with relatively large, regularly shaped patches. (c) Patchy spinel, with diffuse, irregularly shaped patches. (d) Patchy spinel, with Cr-rich patches concentrated in one part of the crystal. (e) Gradational spinel. Cr decreases from upper left to lower right. (f) Chevron spinel. Note the several straight, angular bands of differing Cr contents, which crystallized around a forsterite grain. In (f), (g), and (h), solid lines indicate locations of electron probe traverses. (g) Chevron spinel, in which the bands are parallel to crystal faces. (h) Core-rim spinel, which has a Cr-poor core and several outer Cr-rich bands parallel to crystal faces. The boundary between the core and the Cr-rich spinel is highly irregular and embayed. Al-diop: Aluminous diopside. Fo_x: mole percent forsterite in olivine.

Gradational

In this type, Cr_2O_3 varies fairly smoothly across the grains, by as much as 10 wt%. An example is shown in Fig. 1e. Because these are crystal fragments, and the zoning is not concentric, we cannot be certain that straight edges are crystal faces. If we assume they are, then we can infer core-rim relationships. It appears that in three of the grains, Cr_2O_3 increases toward the rim of the crystal and, in two others, it decreases. In sample SP27, FeO covaries with Cr_2O_3 and ranges from 2.5 to 6 wt%.

Chevron

Six samples fall into this category, in which the grains have as many as ten angular, concentric, sharply defined bands with differing Cr_2O_3 contents (Fig. 1f,g). In this type and the core-rim type (see below), there is concentric zoning, so we can identify the cores and rims of crystals with more confidence than we can for the gradational grains. In at least two cases, including the sample shown in Fig. 1g, the layers are parallel to crystal faces. Band widths range from ~5 to ~30 μm, with typical composition differences of 2–3 wt% Cr_2O_3. One sample, SP44, has a core with ~5 wt% Cr_2O_3, a low-Cr_2O_3 zone (0.4 wt%), and an outermost layer with ~4 wt%. In four other chevron-type grains, the core is relatively low in Cr_2O_3, the layer adjacent to it is the most Cr_2O_3-rich one, and outward from this layer are alternating bands of high and low Cr_2O_3 contents superimposed on a general trend of decreasing Cr_2O_3.

Core-rim

The two grains of this type have low-Cr_2O_3 (1–2 wt%) cores completely enclosed by high-Cr_2O_3 (5–6 wt%) rims.

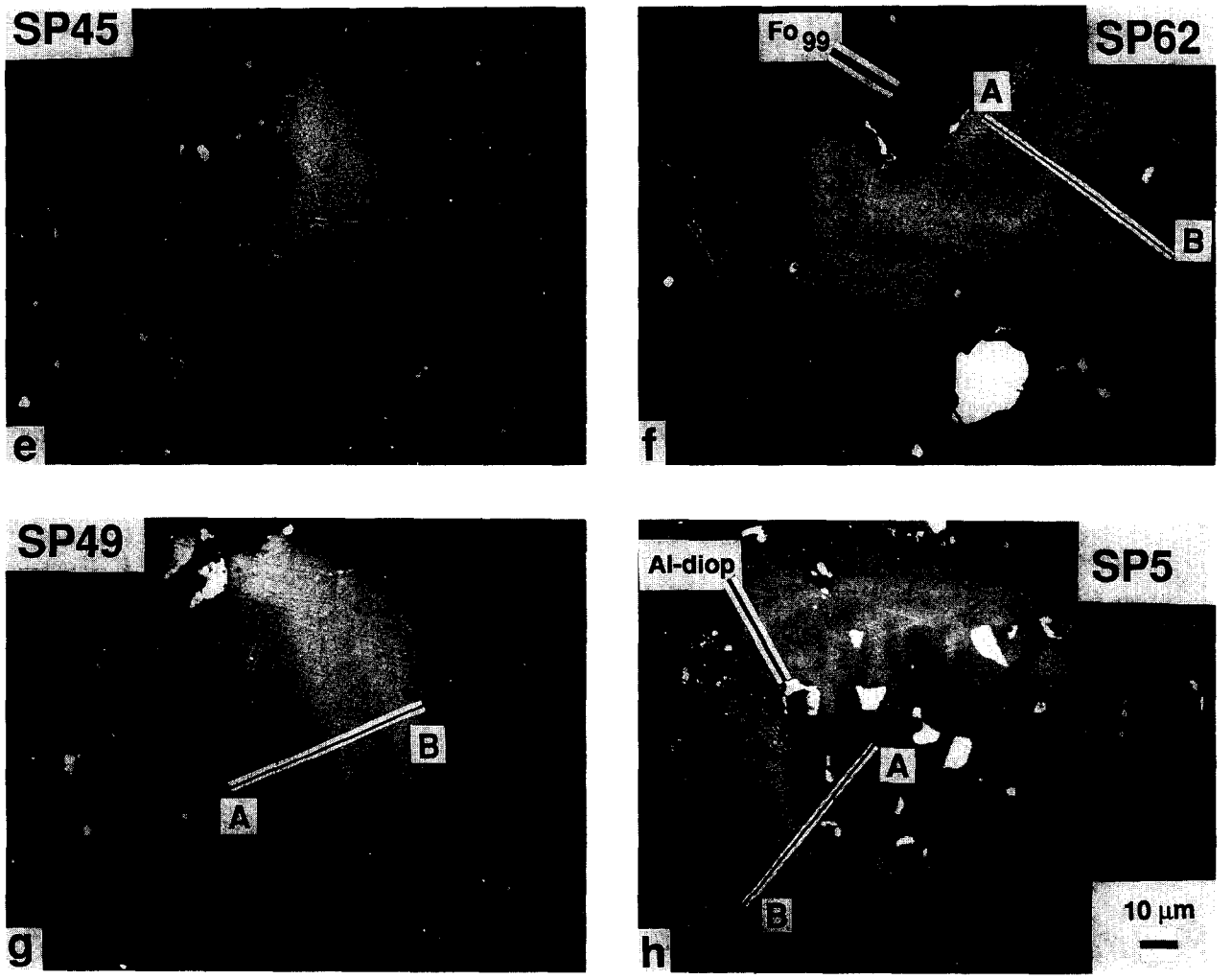

FIG. 1. (Continued)

and, unlike the chevron-type grains, the boundaries between the two zones are irregular and embayed, as in SP5 (Fig. 1h). Like some chevron-type grains, the mantle of SP5 has thin layers of alternating (high and low) Cr_2O_3 contents. The other core-rim sample, SP28, does not have discrete layers in its rim.

In-situ Spinel

Because the freeze-thaw process may have separated most of the spinel grains from any coexisting phases, we have searched optically for occurrences of analogous spinels in their original setting in a total of $\sim 8 \times 10^3$ mm^2 in 40 Murchison thin sections, eight of which were examined in detail by SEM. Despite the large number of spinel grains obtained by freeze-thaw disaggregation, this exhaustive search of thin sections revealed only two grains which fall within both the size and composition ranges of the separated spinel grains. Taking into consideration the mass disaggregated (50–200 g; MACPHERSON et al., 1980), the number of spinel grains recovered (~ 100), and the relatively small mass sampled by a thin section (17 mg), we estimate that there should be 0.3–1.4 spinel grains (100 μm across) per 40 thin sections, roughly consistent with the number we found.

One spinel-bearing inclusion, in section M1, consists of an $\sim 250 \times 100$ μm, patchy, pale pink spinel enclosed on three sides by anhedral olivine and an Fe-rich alteration product (Fig. 2a). One of the olivine-spinel contacts is straight but the other two are curved, with the spinel concave relative to the olivine. The remaining edge is in contact with the matrix of the meteorite. The spinel has inclusions of olivine, aluminous diopside and the Fe-rich alteration product. The olivine contains Cr-bearing, aluminous diopside inclusions up to ~ 10 μm across.

The other occurrence of a large spinel in an inclusion, in section 4377-1 (Fig. 2b), is similar to that in M1, consisting predominantly of coarse, pale pink spinel and anhedral olivine, with the spinel partially enclosing an adjacent olivine crystal. Also, as in M1, there is an Fe-rich alteration product adjacent to both the olivine and spinel. In some places, it appears to have replaced whole lath-shaped crystals. In 4377-1, however, the spinel is homogeneous (not patchy as in M1); the inclusion in 4377-1 contains exsolved high- and low-Ca pyroxene; and the olivine contains inclusions of Ca-rich pyroxene and stringers and isolated blebs of Fe metal in a texture similar to that observed in ureilites (NEUVONEN et al., 1972). There is also Ca-rich pyroxene adjacent to some of the metal blebs. The spinel and olivine grains are ~ 100 μm across but

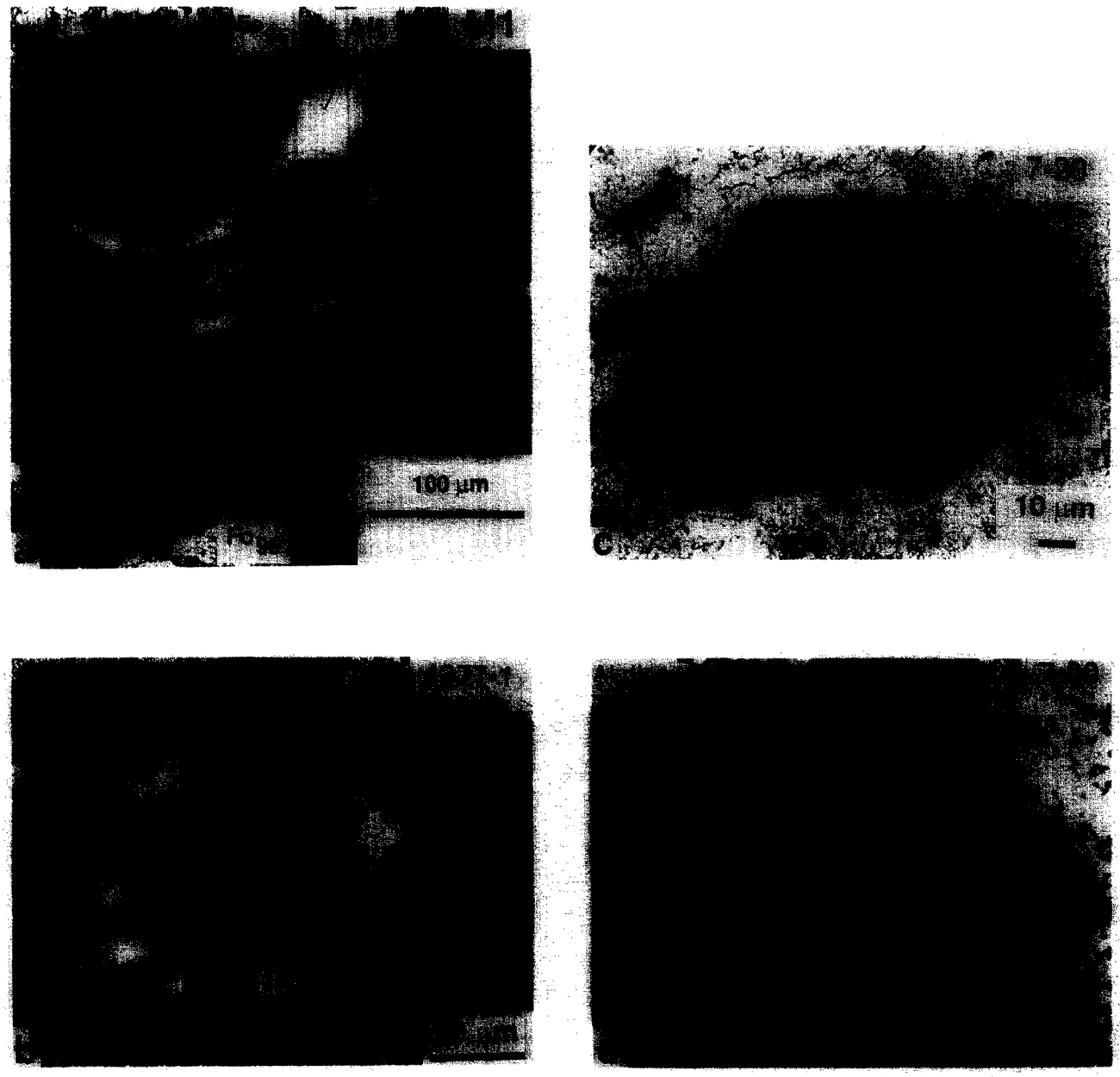

FIG. 2. BEI of in situ spinel. (a) Patchy spinel, partially enclosing olivine grains. (b) Homogeneous spinel, again partially enclosing olivine. (c) Patchy spinel between several olivine grains. (d) Higher-magnification and higher-contrast view of patchy spinel in 2(b). As in M1, there is no obvious relationship between the spinel-matrix contact and the pattern of patches. (e) Chondrule with olivine and homogeneous, gradational, and core-rim spinel in a matrix of aluminous diopside. Most of the olivine nucleated on the edge and grew inward. (f) Chondrule with subhedral to euhedral olivine and homogeneous spinel in a matrix of aluminous diopside. Sp: spinel; cpx: clinopyroxene; Ol: olivine; Al-diop: aluminous diopside; Phy: phyllosilicate; Alt: alteration product; Fo_x: mole percent forsterite in olivine.

the pyroxene is much finer (<20 μm). Neither M1 nor 4377-1 is round, and they probably are fragments of once-larger objects.

In addition to M1, the only other patchy spinel grain which we have found in a thin section of Murchison is a small, 30 × 20 μm grain in sample 7-20 (Fig. 2c,d). As in the in-situ occurrences previously described, the spinel wraps around rounded olivine crystals. In this sample, the spinel is also adjacent to a subhedral olivine crystal that is ~100 × 85 μm and whose contact with the spinel is also curved, but along part of the boundary the olivine curves around the spinel. Aluminous diopside is present between the two smaller olivine crystals and as inclusions in the spinel. The large olivine crystal contains μm-sized blebs of Fe metal. In this sample, as in M1, the patchy spinel is in contact with the matrix of the meteorite, but there is no relationship between these contacts and the patches.

In our density separates, we found a chondrule, M92SP1, 200 μm in diameter, consisting of anhedral to subhedral Cr-bearing spinel (20–50 μm across) and anhedral to euhedral

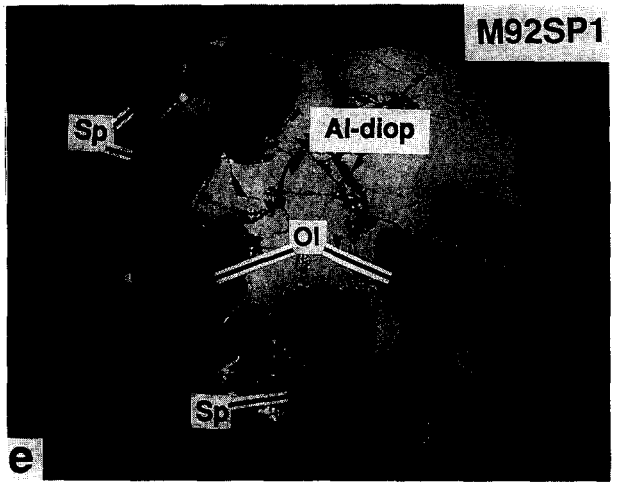

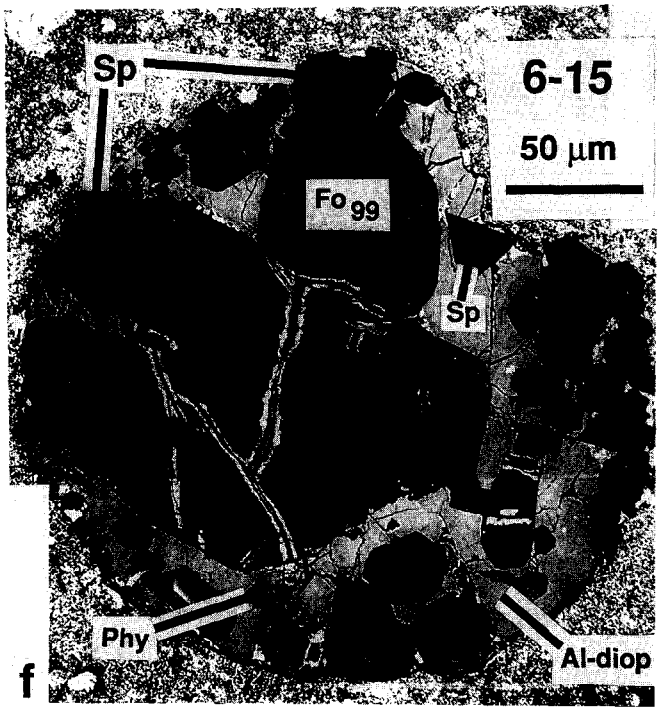

FIG. 2. (Continued)

olivine (30–75 μm long) in a matrix of aluminous diopside (Fig. 2e). Several grains of aluminous diopside are present, the largest being 75 μm across. Most spinel and olivine crystals are at or near the rim, including one spinel grain (at left in Fig. 2e) that has crystallized around olivine, and the olivine grains are oriented at high angles to the surface of the chondrule. One of the spinel grains is homogeneous; two are Cr- and Fe-rich at the surface of the chondrule, becoming less so inward, and are classified as gradational; and two others (at bottom center of Fig. 2e), which have grown together, have low-Cr cores and relatively Cr-rich rims, with smooth boundaries between the zones.

The mineralogy of this chondrule is very similar to one found in thin section, sample 6-15 (Fig. 2f). This sample also contains olivine and spinel in a matrix of aluminous diopside. In addition, it contains phyllosilicate and FeS, and has a higher olivine/pyroxene ratio than M92SP1. The olivine, Fo_{99}, is coarse (25–150 μm) and subhedral to euhedral. Spinel occurs as small, homogeneous grains ~20 μm across, and is also subhedral to euhedral. In one place (at left in Fig. 2f), as in M92SP1, it has crystallized around the end of an olivine crystal, indicating that spinel crystallized after olivine.

Inclusions in Spinel

In addition to their relatively large sizes and various zoning patterns, another distinctive feature of the separated spinel grains is their inclusions. As indicated in Table 1, the most common inclusion by far is aluminous diopside (12–24 wt% Al_2O_3), which occurs in twenty-six grains. Of these, twenty-one have patchy zoning, three have chevron zoning, and two are core-rim grains. The diopside inclusions are anhedral, typically 2–10 μm across and, in many cases, are associated with circular voids, as if pre-existing cavities were partially filled by diopside. There are several exceptions to this mode of occurrence. One grain, SP6, has a 25 μm-thick rind of aluminous diopside which partially encloses both the spinel and an adjacent forsterite grain. Sample SP23 has an irregularly shaped, ~50 μm inclusion, and SP4 has a very thin, discontinuous layer of aluminous diopside between forsterite and the spinel that partially encloses it.

Eleven spinels (seven patchy, two chevron, two homogeneous) occur with olivine, and in all but two of them, SP6 and SP71, spinel partially to completely encloses the olivine, providing clear textural evidence that, in those nine samples, olivine formed before spinel. An example is SP62, shown in Fig. 1f. In six cases (SP4, SP6, SP23, SP62, SP73, and SP79), the olivine is pure forsterite, in one (SP72) it is Fo_{97-98} and in four others (SP50, SP61, SP70, and SP71), it is Fo_{95-96}. The olivine ranges in size from 10 (SP71) to ~100 μm (SP50 and SP70) and in shape from anhedral (SP4, SP23, SP50, SP61, SP71, and SP79) through subhedral (SP62, SP70, SP72, and SP73) to nearly euhedral (SP6). In SP50 and SP61, the olivine contains micrometer-sized blebs of NiFe metal. The olivine in SP50 also has several anhedral, ~5 μm inclusions of Cr-spinel.

Five spinel grains have 5–10 μm-sized inclusions of Ca-, Al-, Si-rich glass. Some are shown in Fig. 3. These glass inclusions tend to be relatively angular, unlike those found in olivine crystals in Murchison (FUCHS et al., 1973; ROEDDER, 1981). Sample SP64 is unusual in that it has a two-phase inclusion consisting of aluminous diopside and glass. Of the five spinels with glass, four have patchy zoning and one has chevron zoning.

Other inclusions observed in spinel are Fe-silicate (probably an alteration product), FeS, FeNi metal, and, in SP66, ~10 μm grains of anorthite or glass of anorthite composition. SP7, SP27, and SP81 contain grains of a Ca-silicate that are too small to identify.

PHASE COMPOSITIONS

Spinel

The suite of separated spinel grains exhibits a wide range of Cr_2O_3 (0.3–37 wt%) and FeO (0.2–17 wt%) contents.

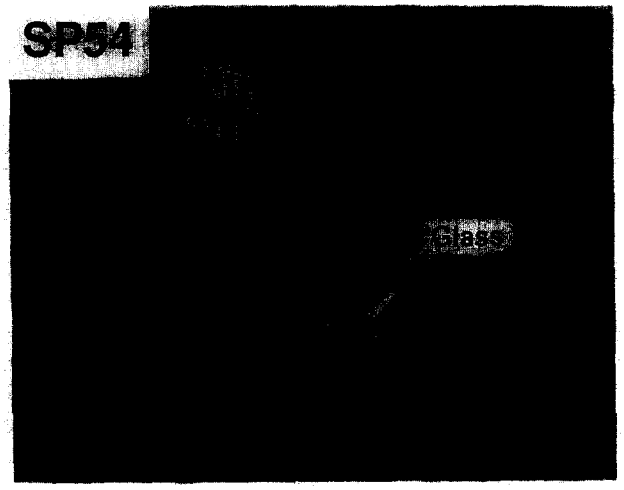

FIG. 3. Glass inclusions in SP54. Note their angular shapes, which are unlike the rounded inclusions found in olivine. Scale bar is 10 μm.

Representative analyses are given in Table 2. So little TiO_2 is present in the spinel that compositions can be represented by (Mg, Fe)(Al, $Cr)_2O_4$ and plotted on the base of the multicomponent spinel prism (e.g., HAGGERTY, 1972). Because many individual crystals have variations in Cr_2O_3 contents but virtually none in FeO, the effective substitutions are simply Fe for Mg and Cr for Al, and not FeCr for MgAl. Nearly perfect anticorrelations between Mg and Fe and between Cr and Al (Fig. 4) are observed, illustrating the dominance of these substitutions over others, such as Cr for Mg.

V_2O_3 ranges from 0.01 to 0.4 wt% and is positively correlated with Cr_2O_3 contents ($r = 0.72$), which is understandable because both elements are compatible in normal spinel (IRVING, 1978). TiO_2 contents are typically 0.2–0.4 wt% and are also correlated with Cr_2O_3 contents, but not as strongly

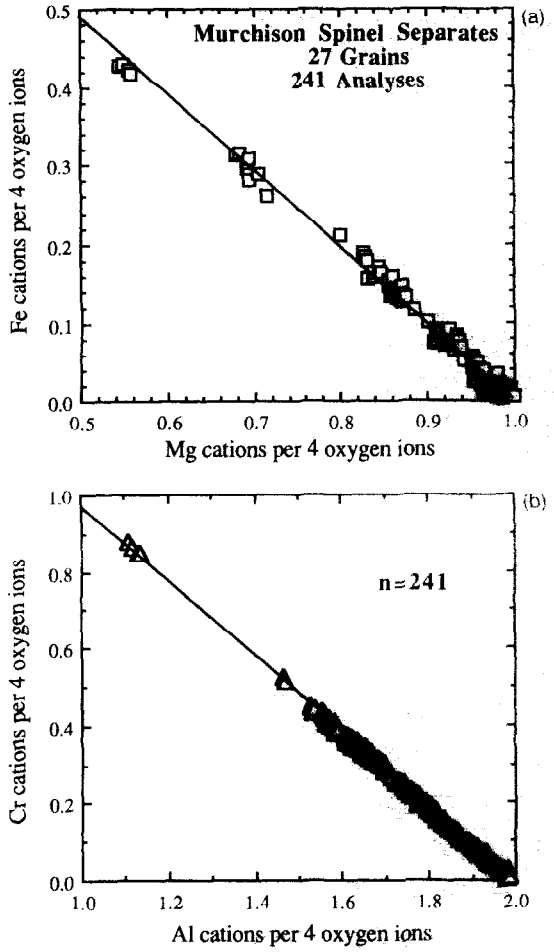

FIG. 4. Summary of Fe-Mg (a) and Cr-Al (b) relationships in electron microprobe analyses of spinel. The best fit lines through the data have slopes very close to −1, showing that these are the dominant substitutions in these spinels.

Table 2. Representative analyses of spinel.

	<-----SEPARATES----->									<-----IN-SITU----->					
	<---Patchy--->				<---Chevron--->			<---Core-Rim--->		<---Patchy--->				Homogeneous	
	SP41 Low-Cr	SP41 High-Cr	SP7 Low-Cr	SP7 High-Cr	SP62 Core	SP62 High-Cr layer	SP62 Low-Cr rim	SP5 Core	SP5 Rim	M1 Low-Cr	M1 High-Cr	7-20 Low-Cr	7-20 High-Cr	4377-1	6-15
MgO	27.61	26.62	17.59	16.95	27.48	26.90	27.94	27.39	27.28	24.00	22.58	26.35	25.72	25.07	28.12
Al_2O_3	68.53	62.73	55.86	52.35	65.63	63.30	68.63	69.92	65.92	55.33	46.85	61.92	54.69	50.42	69.43
SiO_2	0.10	0.08	0.13	0.14	0.23	0.19	0.07	0.06	0.16	0.08	0.08	0.16	0.08	0.10	0.11
CaO	0.01	0.02	0.02	0.02	0.01	BLD	0.01	0.01	BLD	BLD	BLD	0.03	0.02	0.01	0.04
TiO_2	0.22	0.29	0.16	0.16	0.19	0.18	0.14	0.12	0.19	0.28	0.43	0.21	0.27	0.27	0.22
V_2O_3	0.30	0.23	0.18	0.21	0.27	0.31	0.10	0.18	0.20	0.26	0.29	0.26	0.32	0.30	0.18
Cr_2O_3	2.59	8.68	11.94	15.50	6.20	7.15	2.96	1.62	5.31	15.24	23.65	8.67	16.85	22.23	1.92
MnO	BLD	BLD	0.36	0.39	BLD	BLD	BLD	0.01	0.01	0.03	0.03	BLD	BLD	0.20	BLD
FeO	0.34	0.64	13.39	14.00	0.61	0.61	0.45	0.71	0.59	4.37	5.00	1.35	1.44	1.01	0.64
TOTAL	99.70	99.29	99.63	99.72	100.62	98.64	100.30	100.02	99.66	99.59	98.91	98.95	99.39	99.61	100.66
Mg	0.988	0.978	0.693	0.678	0.987	0.990	0.995	0.975	0.986	0.916	0.898	0.975	0.975	0.965	0.996
Al	1.940	1.823	1.740	1.656	1.865	1.842	1.934	1.968	1.885	1.670	1.474	1.812	1.641	1.535	1.945
Si	0.002	0.002	0.003	0.004	0.006	0.005	0.002	0.001	0.004	0.002	0.002	0.004	0.002	0.003	0.003
Ca	0	0	0.001	0	0	0	0	0	0	0	0	0.001	0.001	0	0.002
Ti	0.004	0.005	0.003	0.003	0.003	0.003	0.002	0.002	0.004	0.005	0.009	0.004	0.005	0.005	0.004
V	0.006	0.005	0.004	0.005	0.005	0.006	0.002	0.003	0.004	0.005	0.006	0.005	0.007	0.006	0.003
Cr	0.049	0.169	0.249	0.329	0.118	0.139	0.056	0.031	0.102	0.308	0.499	0.170	0.339	0.454	0.036
Mn	0	0	0.008	0.009	0	0	0	0	0	0.001	0.001	0	0	0.004	0
Fe	0.007	0.013	0.296	0.314	0.012	0.013	0.009	0.014	0.012	0.094	0.112	0.028	0.031	0.022	0.013
Cations/4 ox	2.996	2.995	2.997	2.998	2.996	2.998	3.000	2.994	2.997	3.001	3.001	2.999	3.001	2.994	3.002
Mg/(Mg+Fe)	0.993	0.987	0.701	0.683	0.987	0.987	0.991	0.986	0.988	0.907	0.889	0.972	0.969	0.978	0.987
Cr/(Cr+Al)	0.025	0.085	0.125	0.166	0.060	0.075	0.028	0.015	0.051	0.156	0.253	0.086	0.171	0.228	0.018

BLD: Below limit of detection—0.005 wt % MnO, 0.022 wt % CaO.

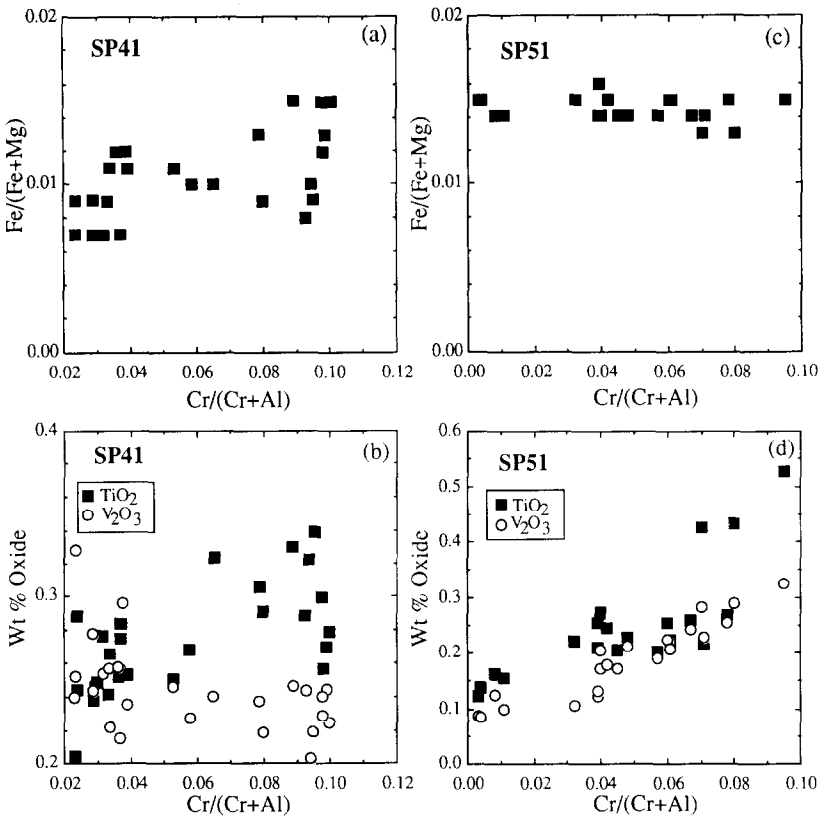

FIG. 5. Plots of atomic Fe/(Fe + Mg) and wt% TiO_2 and V_2O_3 vs. atomic Cr/(Cr + Al) ratios in two patchy spinel grains. (a, b) SP41. (c, d) SP51.

as V_2O_3 is. MnO contents are <0.2 wt% in most spinels, but are ~0.4–0.8 wt% in the two spinels (SP7 and SP52) with >10 wt% FeO. In two other samples, SP49 and SP56, MnO contents are positively correlated with FeO contents. ZnO contents are low (<0.015 wt%) in all samples.

Tables 1 and 2 show that the compositions of the low-Cr and high-Cr patches in the patchy spinels vary from grain to grain. While the FeO contents are typically uniform from patch to patch within individual grains, the observed maximum differences in Cr_2O_3 concentrations between patches range from 1.5 to 12.9 wt% from grain to grain, and average 4.7 wt%. Analyses of the patchy spinels SP41 (Fig. 1a) and SP51 (Fig. 1c) are shown in Fig. 5. In both spinels Cr/(Cr + Al) (henceforth Cr#) ranges from ≤0.02 to ~0.10 but Fe/(Fe + Mg) (henceforth Fe#) has a much narrower range. In SP41, in which most of the contacts between patches are sharp, the Cr# varies continuously, showing no hiatus >0.014. In SP51, in which the contacts are diffuse, a hiatus in Cr# of 0.021 is seen. In SP41 the Cr-rich patches tend to be higher in TiO_2 and lower in V_2O_3 than the low-Cr patches, but there is much overlap between patches in the contents of these oxides. In the patches in SP51, TiO_2 and V_2O_3 contents are positively correlated with Cr#, unlike SP41.

Although individual homogeneous spinel grains have uniform compositions, taken as a group, the homogeneous spinels have a very wide range of Cr_2O_3 contents, from 1.5 to 37 wt% (Table 1). The grain with the most Cr_2O_3, SP52, also has the highest FeO. Individual gradational grains have variations in Cr_2O_3 of up to 10 wt%, and in two of the samples, SP27 and SP42, Fe# covaries with Cr#, as shown in Fig. 6.

Data from electron probe traverses on the chevron grains shown in Fig. 1 are given in Fig. 7. The data for SP62 show that the bands visible in the BEIs (Fig. 1f) are due to variations in Cr#; the Fe# is virtually constant across the grain. In this sample and SP67 (not shown), the outermost layer is very Cr-poor, and TiO_2 and V_2O_3 also drop off sharply. SP49 has

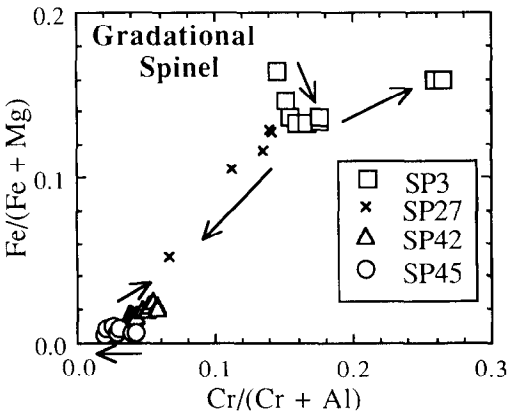

FIG. 6. Plot of atomic Fe/(Fe + Mg) vs. atomic Cr/(Cr + Al) ratios in gradational spinel grains. Arrows point away from the core composition toward the rim composition for each grain. The ratios are correlated in this group overall and within SP42 and SP27.

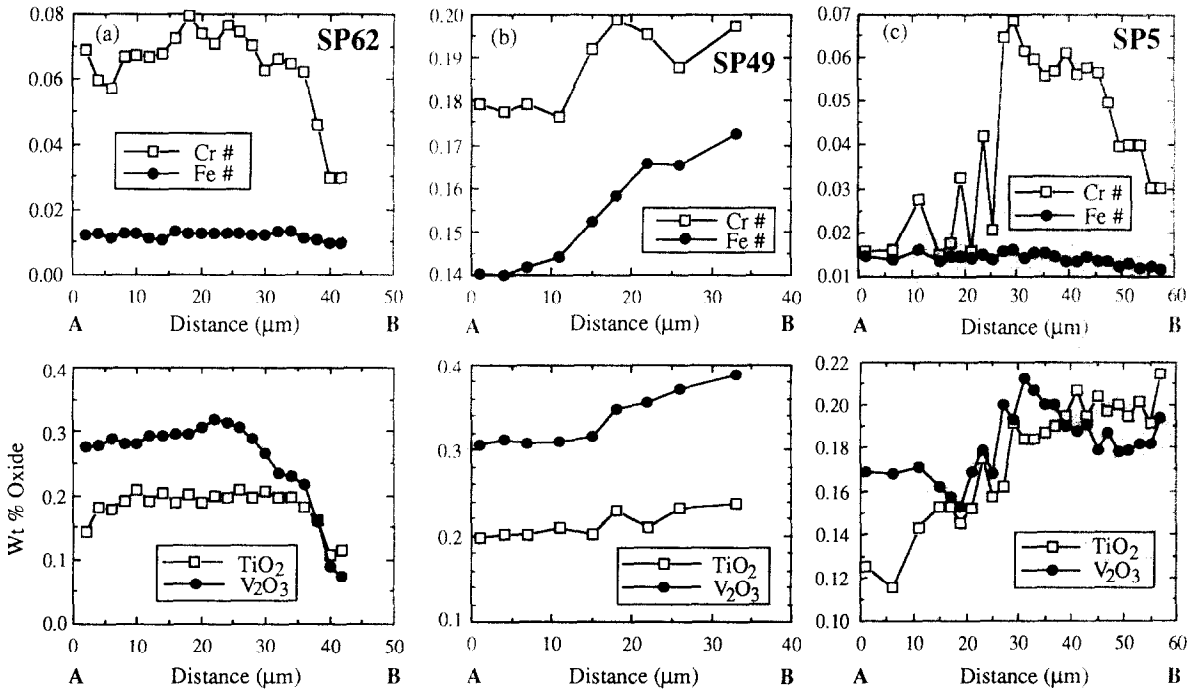

FIG. 7. Results of electron probe traverses for the chevron and core-rim grains shown in Fig. 1. "A" and "B" correspond to the end points of each traverse and are also indicated in Fig. 1. Cr# = atomic Cr/(Cr + Al); Fe# = atomic Fe/(Fe + Mg). (a) SP62, chevron type. Note uniformity of Fe/(Fe + Mg) ratio despite variations in Cr#. (b) SP49, chevron type. Fe/(Fe + Mg) increases from core to rim, while Cr/(Cr + Al) increases, decreases, then increases again. (c) SP5, core-rim type. The data reflect a Cr-poor core enclosed by alternating Cr-rich and Cr-poor layers. Note the high V_2O_3/TiO_2 ratio of the core (0–20 μm) relative to the outer parts of the crystal.

a uniform, low-Cr core and relatively Cr_2O_3-, FeO-, and V_2O_3-rich outer layers. Three layers (light, dark, and light) can be seen in Fig. 1g, and the data from the traverse also show a relatively Cr-poor core (0 to ~10 μm) followed by a relatively Cr-rich layer, a relatively Cr-poor one, and another Cr-rich one. This grain is unusual in that FeO increases from core to rim, whereas most other spinels in this suite have uniform FeO contents. In the data for SP5 (core-rim type), note that the Fe# is ≤0.015 throughout the traverse despite the fluctuations in Cr#, which again correspond to layers visible in the BEI (Fig. 1h). The core has a much higher V_2O_3/TiO_2 ratio than the outer layers.

Among the in-situ samples, the patchy spinel in M1 is Cr-rich, with 15–23 wt% Cr_2O_3, and it has 4.5–5 wt% FeO. FeO and V_2O_3 are positively correlated with Cr_2O_3. In 7-20, FeO, TiO_2, and V_2O_3 are all positively correlated with Cr_2O_3. In chondrule 6-15, the spinel is homogeneous, with 1.9–2.2 wt% Cr_2O_3 and 0.6–0.7 wt% FeO. Spinel in chondrule M92SP1 has 4.5–7.7 wt% Cr_2O_3 and 1.1–2.1 wt% FeO.

Pyroxene

Representative analyses are given in Table 3. Pyroxene associated with the separated spinels is aluminous diopside, with at least 11 wt% Al_2O_3 and up to 3.7% TiO_2. MgO, Al_2O_3, and TiO_2 contents are within the ranges for low-Ti pyroxene from refractory inclusions (Ca-, Al-rich inclusions, or CAIs) in Murchison (MACPHERSON et al., 1983, 1984a), although some of the latter have pyroxene containing higher TiO_2 and Al_2O_3, as does fassaite from Allende Type B CAIs. In SP6, pyroxene forms a partial rind of uniform composition around the spinel. In the other sample (SP23) with pyroxene coarse enough to permit more than one analysis per grain, the pyroxene is also uniform in composition. Almost all pyroxene in the separated spinels has <1 wt% FeO, with the exception of that in SP7. In this sample, spinel has ~14 wt% FeO and pyroxene has 6–8 wt%.

Table 3. Compositions of pyroxene enclosed in spinel or occurring in spinel-bearing assemblages.

	SP5	SP6	SP7	SP23	SP41	SP51	SP53	4377-1	7-20	6-15
MgO	12.41	13.15	10.07	12.01	11.42	21.00	12.39	23.25	14.45	13.19
Al_2O_3	17.29	15.16	14.69	16.80	18.32	11.02	21.47	2.26	15.39	17.44
SiO_2	43.89	42.85	44.86	45.88	42.22	48.96	40.91	55.00	45.79	44.88
CaO	24.08	24.25	21.57	25.33	24.84	16.32	20.93	17.61	23.36	23.48
Cr_2O_3	0.11	0.25	0.66	0.36	1.21	0.27	1.81	0.58	0.43	0.21
TiO_2	0.96	3.66	1.06	0.06	1.84	1.11	0.60	1.36	0.36	1.89
V_2O_3	0.05	0.06	0.06	0.02	0.08	0.02	0.20	0.02	0.05	0.01
MnO	BLD	BLD	0.37	BLD	BLD	BLD	BLD	n.a.	0.01	n.a.
FeO	0.55	0.07	6.85	0.12	0.21	0.71	0.82	1.40	0.58	0.15
TOTAL	99.34	99.45	100.19	100.58	100.14	99.41	99.13	101.48	100.42	101.25
Si	1.598	1.568	1.659	1.647	1.536	1.741	1.491	1.925	1.646	1.597
^{IV}Al	0.402	0.432	0.341	0.353	0.464	0.259	0.509	0.075	0.354	0.403
Tet. Sum	2.000	2.000	2.000	2.000	2.000	2.000	2.000	2.000	2.000	2.000
^{VI}Al	0.341	0.222	0.299	0.358	0.322	0.202	0.413	0.018	0.298	0.328
Mg	0.674	0.717	0.565	0.642	0.619	1.112	0.673	1.212	0.774	0.699
Ca	0.940	0.950	0.854	0.974	0.968	0.622	0.817	0.660	0.899	0.895
Cr	0.003	0.007	0.019	0.010	0.035	0.008	0.052	0.016	0.012	0.006
Ti	0.026	0.101	0.029	0.001	0.050	0.030	0.017	0.036	0.010	0.051
V	0.001	0.002	0.002	0	0.002	0	0.005	0.001	0.001	0
Mn	0	0	0.029	0	0	0	0	---	0	---
Fe	0.017	0.002	0.212	0.004	0.006	0.021	0.025	0.041	0.017	0.005
Oct. Sum	2.002	2.001	2.009	1.989	2.002	1.995	2.002	1.984	2.011	1.984
Cations per 6 ox	4.002	4.001	4.009	3.989	4.002	3.995	4.002	3.984	4.011	3.984

BLD: below limit of detection of 0.005 wt % MnO. Sc_2O_3 was BLD (0.005 wt %) in all pyroxene analyzed. n.a.: not analyzed

Pyroxene included in and occurring with in-situ spinel is also mostly aluminous diopside, with the exception of 4377-1, which has both high- and low-Ca pyroxene with only ~2 wt% Al_2O_3, in contrast to the ~17% that is typical of the pyroxene found included in the separated spinels and occurring with the other in-situ spinels.

Olivine

Analyses of olivine occurring with spinel are given in Table 4. Among the separated spinel grains, there is a bimodal distribution of olivine compositions. With the exception of two samples, spinel either occurs with pure forsterite ($Fo_{>99}$) or with $Fo_{95\text{-}96}$. The pure forsterites all have high (~1 wt%) CaO contents, whereas the grains with more FeO tend to have lower CaO but higher MnO and Cr_2O_3 contents than the former (Fig. 8).

Also shown in Fig. 8 are analyses of olivine that occurs with in-situ spinel. Unlike the unzoned olivine in the separates, some olivine in the in-situ occurrences is weakly zoned. The largest crystal in 4377-1 is zoned from Fo_{98} to Fo_{99}, and the large subhedral grain in 7-20 is reversely zoned, from $Fo_{95.5}$ to $Fo_{97.8}$. The latter olivine is relatively rich in CaO (0.6–0.7 wt%). Cr_2O_3 contents are high and tend to increase with FeO, but MnO contents are low and increase slightly with FeO. In 4377-1, the olivine has high Cr_2O_3 and MnO contents and low CaO. MnO is anticorrelated with FeO, consistent with loss of iron by reduction (MIYAMOTO et al., 1993). Analyses of the other samples plot along the normal MnO-FeO trend for olivine from CM2 chondrites (STEELE, 1990). Olivine in M1 has Cr_2O_3 contents which range from ~0.4 to 0.8 wt% and do not covary with FeO or MnO. In the chondrules (6-15 and M92SP1), olivine has ~1–2 wt% FeO, very low MnO, and lower CaO than the pure forsterite found with some of the spinel in the separates.

Table 4. Compositions of olivine occurring with spinel.

	SP4	SP50	SP61	SP62	M1	4377-1
MgO	55.03	51.85	53.53	56.45	53.14	56.50
Al_2O_3	0.54	0.28	0.32	0.30	0.10	0.12
SiO_2	42.26	41.01	41.80	41.80	41.73	41.92
CaO	0.77	0.27	0.29	1.03	0.30	0.24
TiO_2	0.07	0.06	0.07	0.06	0.04	0.08
V_2O_3	0.05	0.02	0.03	0.03	0.02	0.02
Cr_2O_3	0.46	0.57	0.65	0.24	0.63	0.61
MnO	BLD	0.09	0.07	BLD	0.05	0.19
FeO	0.31	5.23	3.88	0.64	4.26	1.06
TOTAL	99.49	99.39	100.64	100.55	100.27	100.74
Si	0.999	0.992	0.992	0.982	0.996	0.984
Mg	1.938	1.870	1.894	1.976	1.890	1.976
Al	0.015	0.008	0.009	0.008	0.003	0.003
Ca	0.019	0.007	0.007	0.026	0.008	0.006
Ti	0.001	0.001	0.001	0.001	0.001	0.001
V	0.001	0	0	0.001	0	0
Cr	0.009	0.011	0.012	0.005	0.012	0.011
Mn	0	0.002	0.001	0	0.001	0.004
Fe	0.006	0.106	0.077	0.013	0.085	0.021
Total cations/4 ox	2.988	2.997	2.993	3.012	2.996	3.006
mole % Fo	99.7	94.6	96.1	99.3	95.7	98.9

BLD: below limit of detection of 0.004 wt % MnO. NiO and Sc_2O_3 were looked for but not detected.

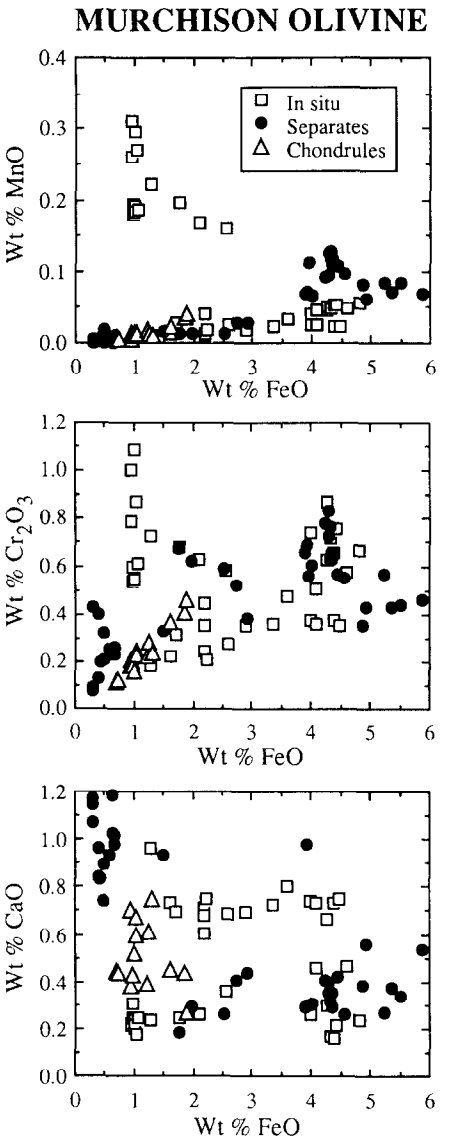

FIG. 8. Plots of MnO, Cr_2O_3, and CaO vs. FeO contents in olivine associated with spinel.

Glass

Five spinel grains have inclusions of Si-, Al-, Ca-rich glass (Table 5). Four of the spinels are patchy and one has chevron-type zoning. The glasses are generally similar to, but have less MgO than, glass inclusions found in isolated olivine crystals in Murchison (FUCHS et al., 1973) whose average composition is also given in Table 5. The glasses found in spinel also bear some similarity to glasses found in ferromagnesian chondrules in ordinary chondrites (JONES and SCOTT, 1989; JONES, 1992), but the glasses reported here have lower MgO and Na_2O contents than chondrule glass.

Other Associated Phases

Many of the spinel grains either enclose or are attached to small amounts of Fe-rich silicate, analyses of which are given in Table 6. Low totals indicate that it is a hydrous phase and,

Table 5. Compositions of glass inclusions in Murchison spinels.

	SP44	SP54	SP63	SP64	Olivine*
MgO	3.35	1.92	2.45	2.91	4.2
Al_2O_3	22.85	24.84	23.47	23.73	21.6
SiO_2	47.95	52.38	53.47	61.02	52.1
CaO	23.41	20.32	18.18	12.91	18.1
TiO_2	1.84	0.96	0.36	0.71	0.8
V_2O_3	0.05	0.05	0.36	BLD	n.a.
Cr_2O_3	0.44	0.44	0.47	0.21	0.2
MnO	n.a.	0.02	0.08	0.02	0.03
FeO	0.30	0.28	0.58	0.61	1.3
TOTAL	100.19	101.21	99.42	102.12	

n.a.: not analyzed. BLD: below limit of detection of 0.005 wt % V_2O_3.
*Average of eleven analyses of glass in isolated olivine crystals (FUCHS et al., 1973).

in some cases, is similar in composition to that found in Murchison CAIs (MACPHERSON et al., 1984a). The phyllosilicates in SP71 and SP78 are fairly S-rich, however, and are probably mixtures of cronstedtite, serpentine, and an Fe-, S-, O-, Ni-bearing phyllosilicate found in CM2 matrices (TOMEOKA and BUSECK, 1985).

ISOTOPIC COMPOSITION OF SPINEL

Oxygen

The oxygen isotopic compositions measured in the Burma spinel standard and twelve separated spinel grains are given in Table 7 and are plotted in Fig. 9, along with those of spinel-rich acid residue 2C10c (CLAYTON and MAYEDA, 1984) and the average of nine Mg-, Al-rich spinel grains from acid residue CFOc (VIRAG et al., 1991), both from Murchison. In the oxygen 3-isotope diagram, the spinel samples from the present study plot in a cluster close to the intersection of the terrestrial fractionation line and the unit slope mixing line for refractory phases from carbonaceous chondrites (CLAYTON et al., 1977). The scatter of the oxygen isotopic compositions measured on different standard grains (Table 7) considerably exceeds the precision of single analyses, probably reflecting variations in the geometry of individual grains. The errors given in Table 7 express only the error of the mean of numerous measurements on each grain, and are smaller for the Murchison spinels because more measurements were made on each grain of the latter. An uncertainty corresponding to the grain-to-grain variation of the Burma spinel data points must be superimposed on the Murchison spinel data. The scatter of Murchison data points is comparable to that shown by those obtained from individual Burma spinel grains. The Murchison spinel data points are thus compatible with a single oxygen isotopic composition.

Table 6. Compositions of Fe-rich alteration products.

	SP70	SP71	SP78	M1	4377-1
MgO	10.19	16.83	7.15	5.59	7.00
Al_2O_3	2.99	5.22	3.85	2.95	4.98
SiO_2	25.32	25.39	13.52	22.48	23.93
CaO	0.40	0.70	0.25	0.04	0.05
P_2O_5	BLD	0.05	0.07	BLD	BLD
SO_3*	0.08	7.82	15.42	0.16	0.43
TiO_2	0.09	0.10	0.06	0.04	0.07
Cr_2O_3	0.68	0.41	2.01	0.98	0.59
FeO	49.85	30.88	48.85	53.67	49.78
NiO	BLD	1.23	2.02	BLD	BLD
TOTAL	89.61	88.63	93.20	85.91	86.83

*S reported as SO_3 but its oxidation state is unknown.
BLD: below limit of detection—0.021 wt % for P_2O_5; 0.057 wt % NiO.

Table 7. Oxygen isotopic compositions of individual grains of the Burma spinel standard and separated Murchison spinels (‰ relative to SMOW)

	$\delta^{17}O \pm 2\sigma$	$\delta^{18}O \pm 2\sigma$
Burma		
1	14.2 ± 4.8	20.7 ± 5.2
2	8.2 ± 5.2	22.9 ± 4.8
3	13.9 ± 6.6	10.2 ± 5.8
4	6.3 ± 5.0	17.0 ± 4.8
5	10.3 ± 6.4	10.6 ± 6.0
6	13.7 ± 5.4	26.7 ± 4.0
7	11.9 ± 5.8	23.7 ± 4.6
8	8.8 ± 6.2	20.5 ± 3.8
9	11.6 ± 4.6	20.0 ± 4.6
10	15.9 ± 5.0	24.3 ± 3.6
11	11.8 ± 6.8	22.4 ± 3.6
12	13.9 ± 4.2	23.0 ± 4.6
13	16.6 ± 5.2	30.8 ± 4.4
14	10.1 ± 5.8	9.6 ± 5.0
15	11.1 ± 6.2	19.7 ± 4.8
16	13.4 ± 4.0	25.3 ± 4.8
17	16.1 ± 4.6	21.1 ± 4.6
18	14.3 ± 6.6	22.7 ± 4.8
19	8.4 ± 5.6	18.7 ± 5.4
20	9.2 ± 4.8	27.1 ± 5.6
21	8.5 ± 4.6	21.5 ± 4.6
22	4.4 ± 4.8	21.4 ± 5.2
Murchison		
SP21	-1.1 ± 4.2	2.3 ± 3.3
SP22	-2.3 ± 3.0	-1.5 ± 4.0
SP24	-0.5 ± 3.0	0.9 ± 3.4
SP27	2.6 ± 4.6	6.9 ± 5.2
SP28	1.3 ± 3.5	0.5 ± 3.2
SP29	-4.0 ± 2.8	-2.1 ± 2.8
SP30	-0.1 ± 3.4	5.0 ± 4.3
SP31	-2.0 ± 3.8	5.2 ± 3.8
SP32	2.9 ± 3.8	5.1 ± 6.0
SP33	-4.5 ± 3.9	-5.9 ± 6.3
SP34	1.3 ± 3.9	7.7 ± 5.2
SP36	-0.4 ± 4.6	5.8 ± 3.9

The nominal composition of Burma spinel is $\delta^{17}O_{SMOW} = 11.6‰$; $\delta^{18}O_{SMOW} = 22.3‰$.

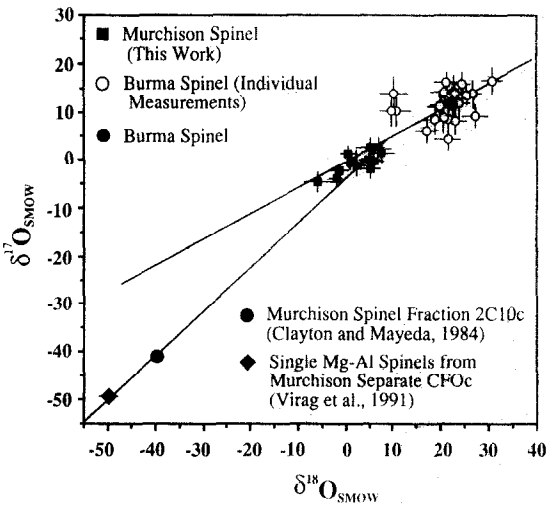

FIG. 9. Oxygen isotopic compositions of Murchison spinels. Analyses of the Burma spinel standard are also given. The stippled circle represents the average of the individual Burma spinel analyses. The solid diamond represents the average of nine spinels from acid residue CFOc. The spinels analyzed for this study have oxygen isotopic compositions that plot on or near the terrestrial fractionation line, unlike those found in acid residues 2C10c and CFOc.

What is most striking is that this composition is essentially normal, in pronounced contrast to the ^{16}O-rich compositions found in Mg-, Al-rich spinel from Allende and Vigarano inclusions (CLAYTON et al., 1977; ZINNER et al., 1991), in the spinel-rich acid residue, 2C10c, from Murchison (CLAYTON and MAYEDA, 1984), in individual spinel grains from another Murchison acid residue, CFOc (MCKEEGAN, 1987; VIRAG et al., 1991), and in hibonite and corundum samples from Murchison (FAHEY et al., 1987; VIRAG et al., 1991; IRELAND et al., 1992).

Previous indications of a wide range of oxygen isotopic compositions of Murchison spinel come from ion microprobe studies of individual spinel grains from the CFOc acid residue. ZINNER and EPSTEIN (1987) reported $\delta^{18}O$ values ranging from +9 to −55‰ from individual Mg-spinel grains identified on the basis of qualitative analysis of energy-dispersive X-ray spectra. MCKEEGAN (1987) used energy-dispersive spectra to distinguish spinel from chromite grains in this residue and measured both $\delta^{18}O$ and $\delta^{17}O$ in individual grains. Most of the grains lie along the unit-slope oxygen isotope mixing line, with some individual spinel grains plotting at lower $\delta^{18}O$ and some at higher $\delta^{18}O$ values than that of the bulk acid residue 2C10c of CLAYTON and MAYEDA (1984). The only chromite grain reported by MCKEEGAN (1987) plots at $\delta^{18}O = -22$, much closer to the terrestrial fractionation line than all of the Mg-spinel grains except one. The CFOc grains whose oxygen isotopic compositions were measured by VIRAG et al. (1991) were selected to be Mg-, Al-spinel by energy-dispersive spectra, and their Cr and Fe concentrations, 80–1500 and 500 ppm, respectively, were measured by ion microprobe. Not included in the average of the spinel grains from CFOc in Fig. 9 is one data point that plots at $\delta^{18}O = 0$‰, in the region of the spinels of the present study (see Fig. 2b of VIRAG et al., 1991). It is noteworthy that the Cr and Fe concentrations in this grain, 4050 and 6100 ppm, respectively (A. Virag, pers. commun.), are substantially higher than in the other CFOc grains, and within the ranges of the spinel grains of the present study.

Chromium

Results for ^{53}Cr and ^{54}Cr abundances are reported in Table 8 as ϵ-unit (parts in 10^4) deviations from the terrestrial normal compositions reported by PAPANASTASSIOU (1986). The data are also plotted in Fig. 10. Within rather variable error limits

Table 8. Cr isotopic data for Murchison spinels.

Sample	N[a]	χ^2_{53}[b]	χ^2_{54}[b]	ε_{53}[c]	ε_{54}[c]
Reagent Cr	31	1.1	1.0	1.3±0.8	5.4±1.4
Burma Spinel	8	1.3	0.5	-0.5±2.0	-1.5±3.8
SP27	2	1.2	5.4	3.0±2.6	1.7±5.4
SP28	5	1.7	0.8	3.3±1.8	4.2±3.8
SP29	2	0.1	0.5	2.1±5.2	-11.3±10.4
SP30	2	0.4	0.4	-2.5±3.4	-3.4±5.8
SP31	13	1.7	1.4	-0.6±1.0	2.5±2.0
SP34	6	1.7		-3.4±2.4	-10.2±10.2

(a) Number of runs for given sample.
(b) Reduced chi-squared for individual runs relative to their mean.
(c) Deviation from terrestrial normal ($^{53}Cr/^{52}Cr = 0.113459$, $^{54}Cr/^{52}Cr = 0.0282129$) of PAPANASTASSIOU (1986), in parts per 10^4; stated errors are two-sigma deviations of the mean of all runs (see text for probable limitations on formal convergence of the mean).

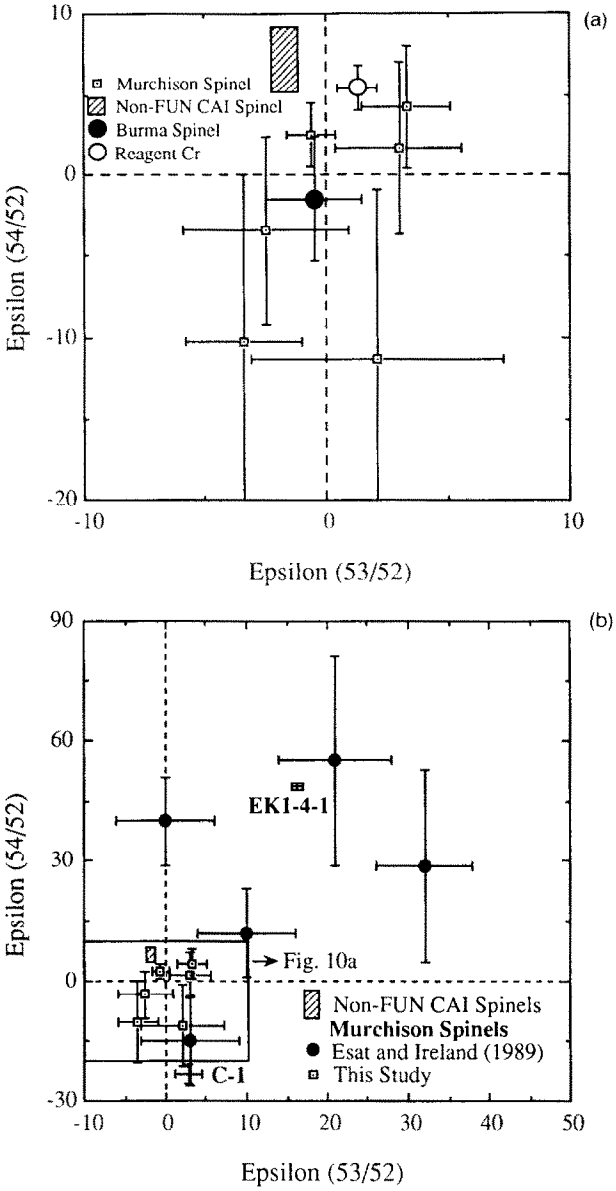

FIG. 10. (a) Chromium isotopic compositions of Murchison spinel, non-FUN CAI spinel (PAPANASTASSIOU, 1986; BIRCK and ALLÈGRE, 1988), and Cr standards. (b) Chromium isotopic compositions of Murchison spinel analyzed by ESAT and IRELAND (1989) and, for reference, compositions in FUN inclusions C-1 and EK 1-4-1 (PAPANASTASSIOU, 1986). The anomalous ratios determined by ESAT and IRELAND (1989) are not observed in the samples studied here.

the data for the individual Murchison spinel grains are consistent, or very nearly so, with normal chromium isotopic composition. It is evident that these data do not support any arguments for isotopic anomalies in chromium in these spinels. The data indicate that chromium in these spinels is isotopically uniform, within less than one ‰.

DISCUSSION

Origins and Sources

Homogeneous and gradational grains

Spinel grains of these types are found in igneous settings. EL GORESY et al. (1971), for example, illustrated gradational

zoning in very Ti-, Cr-rich spinel grains in Apollo 12 basalts. In addition, chondrules crystallized from liquids, and our observation of homogeneous spinel in two chondrules (Fig. 2e, f) suggest chondrules are a possible source for this type of spinel, even though the spinel grains in the chondrules are smaller than the separated spinels. In SP61 and SP73, the two homogeneous spinel samples that occur with olivine, there is clear textural evidence that olivine crystallized before spinel. Igneous crystallization of spinel after olivine might appear to be a problem because most chondrules have very high normative olivine contents and, in melts with these compositions, olivine is typically followed in the crystallization sequence by pyroxene or chromite, but not Mg-, Al-, Cr-spinel. The mineralogy and textures of two spinel-bearing chondrules from Murchison, M92SP1 (Fig. 2e) and 6-15 (Fig. 2f), indicate, however, that liquids did exist from which spinel could crystallize after forsteritic olivine. Both of these chondrules contain spinel crystals that grew around the end of an olivine crystal, and a fragment with a similar texture was found in the separates. The similarity of these occurrences is evident from the close-up views in Fig. 11. To better understand these chondrules, we calculated their bulk compositions from the average mineral compositions and their abundances, and the results are given in Table 9. Note that the compositions are Al_2O_3-rich and FeO-poor relative to those of typical chondrules in CM2 chondrites (column 3 in Table 9), which average ~2 wt% Al_2O_3 and ~14 wt% FeO (OSBORN et al., 1974). These features of the compositions of the latter chondrules cause their residual liquids at the end of olivine crystallization to be Al_2O_3-poor and FeO-rich, and chromite, not aluminous spinel, follows olivine (e.g., JOHNSON and PRINZ, 1991).

Phase equilibria clarify why, in M92SP1 and 6-15, aluminous spinel crystallized after olivine. For early stages of crystallization, we refer to Fig. 12a, which shows the relations for the 15 wt%-Al_2O_3 plane in the CaO–MgO–Al_2O_3–SiO_2 (CMAS) system, because the composition of M92SP1 falls on this plane, and the composition of the residual liquid in 6-15 enters this plane after 45% crystallization of olivine. The samples plot low in the forsterite field. Crystallization of forsterite from melts with these compositions would enrich the residual liquids in Al_2O_3 and drive their compositions

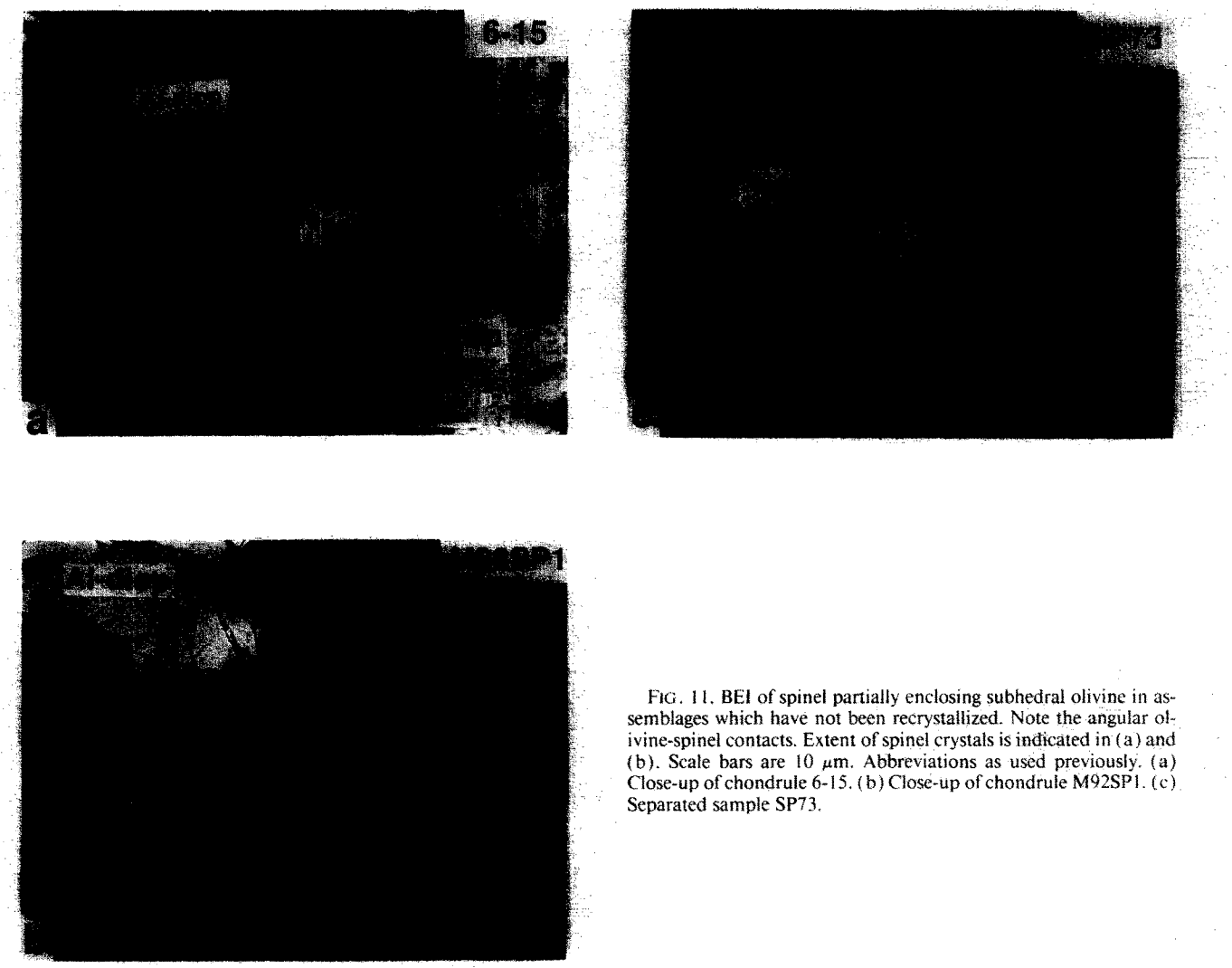

FIG. 11. BEI of spinel partially enclosing subhedral olivine in assemblages which have not been recrystallized. Note the angular olivine-spinel contacts. Extent of spinel crystals is indicated in (a) and (b). Scale bars are 10 μm. Abbreviations as used previously. (a) Close-up of chondrule 6-15. (b) Close-up of chondrule M92SP1. (c) Separated sample SP73.

Table 9. Bulk compositions of chondrules.

	6-15	M92SP1	C2 chondrules[1]	RC071[2]	RC072[2]	ALHA 77299[3]
Na_2O	n.a.	n.a.	0.1	2.8	5.9	3.4
MgO	44.0	35.4	n.a.	14.1	4.4	8.3
Al_2O_3	8.5	15.9	1.9	20.5	24.0	22.8
SiO_2	40.2	37.0	39.2	37.8	47.6	43.4
CaO	5.9	8.8	n.a.	3.2	4.2	8.7
TiO_2	0.4	0.5	n.a.	0.8	1.3	1.3
Cr_2O_3	0.3	1.3	0.5	3.2	2.9	0.9
FeO	0.7	0.8	13.6	10.6	5.8	8.7

n.a.: not analyzed.

[1]Average of INAA analyses of 77 chondrules from several C2 chondrites (OSBORN et al., 1974).

[2]Broad-beam electron probe analysis of Cr-spinel-bearing chondrule in Roosevelt County L chondrites (MCCOY et al., 1991). They also reported 6.7 wt % FeNi in RC 071.

[3]Broad-beam electron probe analysis of a spinel-bearing chondrule (#20) from ALHA 77299, an H3 chondrite (BISCHOFF and KEIL, 1983).

directly away from forsterite toward the forsterite-spinel cotectic, as shown by the arrows through the data points in Fig. 12a. With increasing Al_2O_3 contents in the system, the spinel field expands, effectively causing the forsterite-spinel cotectic to move to the right in Fig. 12a. The dashed lines in the forsterite field give the approximate locations of the forsterite-spinel cotectic at 16, 17, and 18 wt% Al_2O_3 and are labelled accordingly. For M92SP1, crystallization of only ~10 wt% forsterite yields a residual liquid with ~17.5 wt% Al_2O_3, where it reaches the spinel-forsterite cotectic. The residual liquid composition in 6-15 shown in Fig. 12a reaches spinel saturation after crystallization of an additional 7 wt% olivine.

Figure 12b is the gehlenite–anorthite–forsterite plane in CMAS, projected from spinel according to the method of STOLPER (1982). On it we plot the compositions of residual liquids in M92SP1 and 6-15 from which spinel should begin to crystallize. As shown by the lines through the data points in Fig. 12b, the equilibrium phase relations indicate that forsterite + spinel should be joined first by anorthite and then by pyroxene. From the petrography of the chondrules, however, we know that pyroxene followed forsterite + spinel. Apparently the crystallization of anorthite was suppressed and crystallization of forsterite + spinel continued until the liquid composition reached a metastable extension (dashed line in anorthite field) of the pyroxene–forsterite–spinel cotectic. This situation is analogous to late-stage crystallization in some Type B CAIs, in which melilite + spinel crystallization proceeded until a metastable extension of the melilite–pyroxene–spinel cotectic was encountered (MACPHERSON et al., 1984b), causing pyroxene to crystallize before anorthite. YANG (1975) found that pyroxene crystallizing at invariant point *R* on Fig. 12b contains ~20% Al_2O_3, while A. H. Treiman (pers. commun.) found an average of 11.5% Al_2O_3 in pyroxene that crystallized at invariant point *Q*, suggesting that virtually all pyroxene crystallizing in this system is highly aluminous. While it is unclear how anorthite supersaturation will affect the Al_2O_3 content of pyroxene forming along the metastable extension of the pyroxene–forsterite–spinel cotectic, values approaching 17%, like the Al_2O_3 contents of the pyroxene in chondrules 6-15 and M92SP1, do not seem unreasonable.

We have also observed gradational-type spinel grains in a chondrule (Fig. 2e, upper left), as did BISCHOFF and KEIL (1984) and MCCOY et al. (1991) who reported subhedral to euhedral, gradational-type spinel grains ~100 μm across that appear to have nucleated at the margins of Al-rich chondrules in ordinary chondrites. The FeO and Cr_2O_3 contents of these spinel grains decrease with increasing distance from the crystal edge nearest the chondrule rim. Similarly, in two of the separated spinels with gradational-type zoning, SP27 and SP42, FeO increases with increasing Cr_2O_3. Both MCCOY et al. (1991) and BISCHOFF and KEIL (1984) attributed the observed zoning to fractional crystallization. Based on their

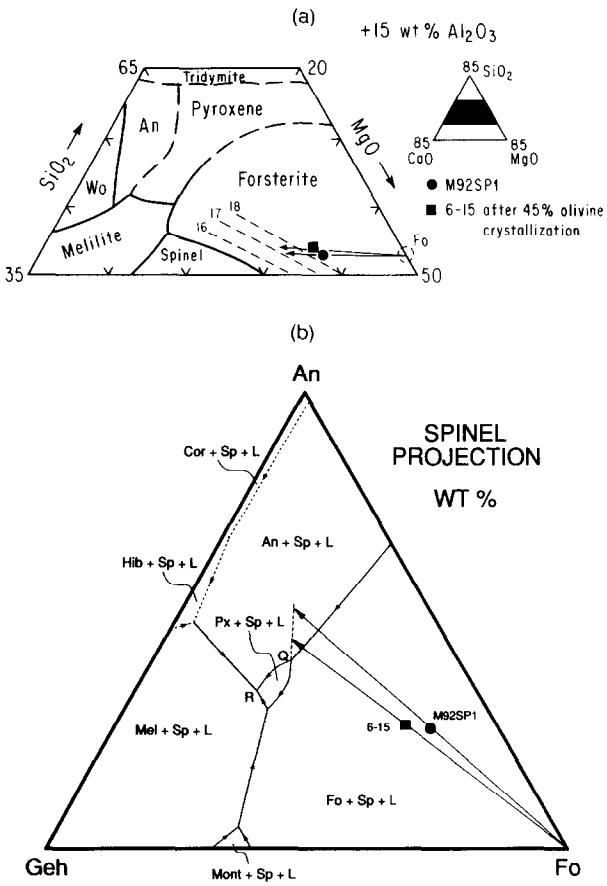

FIG. 12. (a) Part of the 15 wt%-Al_2O_3-plane in CMAS. Compositions of Murchison spinel-bearing chondrules 6-15 (after 45% crystallization of olivine) and M92SP1 are shown, as are the approximate locations of the forsterite-spinel cotectic at different bulk Al_2O_3 contents, showing how the spinel field expands with increasing Al_2O_3. As the chondrules crystallize olivine, the composition of the residual liquid moves toward the forsterite-spinel cotectic, as indicated by the arrows from forsterite (Fo) through the data points. An: anorthite. Wo: wollastonite. After OSBORN et al. (1954). (b) Projection, in weight percent, from spinel onto the gehlenite-anorthite-forsterite plane in the system CaO–MgO–Al_2O_3–SiO_2. Two Al-rich Murchison chondrules (see text) plot in the forsterite field. Crystallization of forsterite plus spinel drives residual liquid compositions away from the forsterite apex into the anorthite field (lines from Fo through data points). Absence of anorthite from these chondrules suggests that anorthite crystallization was kinetically delayed and forsterite crystallization continued until a metastable extension (dashed line, no arrows) of the pyroxene-forsterite cotectic was encountered. Sp: spinel; Fo: forsterite; An: anorthite; Cor: corundum; Hib: hibonite; Px: pyroxene; Geh: gehlenite; Mel: melilite; Mont: monticellite; L: liquid. *R* and *Q* are invariant points discussed in the text. After STOLPER (1982).

coarse, euhedral nature, the spinel crystals in these chondrules formed early, probably nucleating on the edges of the chondrules and growing inward, resulting in their asymmetric zoning. If the gradational-type spinel grains in our suite are representative of complete crystals, then it is likely that they formed in a similar way, i.e., by nucleation on the surface of a chondrule or on another grain in a chondrule, followed by growth away from the attached edge. Bulk compositions of these three gradational spinel-bearing chondrules are given in Table 9 (columns 4–6). It is interesting to note that these chondrules in which spinel crystallizes early, if not first, have higher Al_2O_3 contents (>20 wt%) than M92SP1 and 6-15, in which olivine crystallized first. As suggested by the expansion of the spinel field at the expense of the forsterite field shown in Fig. 12a, increasing Al_2O_3 contents in chondrules of these compositions increase the probability that spinel crystallizes before forsterite. If our proposed origins for the separated homogeneous and gradational spinels are correct, then it is likely that the gradational spinels came from chondrules that were more Al_2O_3-rich than the source chondrules of the homogeneous spinels.

An argument against chondrules being a source of the homogeneous and gradational spinels, however, is the difference in size between those in the separates and those in the chondrules. The homogeneous and gradational spinel grains studied here range from 50 to 180 μm in diameter, with an average of 100 μm, while the largest spinel we have seen in a chondrule is 45 μm. The discrepancy in size is greater than this, since most of the separated grains in this study are fragments of even larger crystals. The spinel-bearing chondrules discussed above are themselves ~7–15 times the average spinel size. If the same were true for the putative parent chondrules of the separated spinels, those chondrules would have to have been in excess of 1.3–2.7 mm in diameter to account for the largest spinel crystals. Chondrules that contain coarse, Al-rich, Cr-bearing spinel grains are exceedingly rare in Murchison, as are chondrules of this size. OLSEN and GROSSMAN (1978) found that Murchison chondrules range in diameter from 175 to 1081 μm, with a mean of only 420 μm. The minimum chondrule size necessary to account for the largest homogeneous and gradational spinel grains in our separates is thus 16% larger than the largest chondrule reported from Murchison, and the average separated spinel would probably require a parent chondrule equal in size to the largest chondrule seen in Murchison. If the homogeneous and gradational spinel grains in the separates originated in chondrules, it is clear that those chondrules are from a population that is not only more aluminous but also much larger on average than that seen in Murchison. Inclusions M1 and 4377-1 do not have round shapes, so it could be argued that they may be remnants of such chondrules.

Core-rim grains

Concentrically zoned spinel grains were reported from Apollo 12 basalts by EL GORESY et al. (1976). They are much more Ti- and Cr-rich than those seen here and their cores are either idiomorphic or rounded, in contrast to the irregular, embayed cores in the grains studied here. This type of grain occurs in chondrule M92SP1 (Fig. 2e, bottom) and in some plagioclase-olivine inclusions in the C3 chondrites Allende (SHENG et al., 1991) and Ninqiang (A. M. Davis, pers. commun.). The grains in M92SP1 have irregularly shaped Mg-poor cores with diffuse core-rim boundaries; those among the separated grains and those described by SHENG et al. (1991) have sharp, corroded core-rim boundaries. SHENG et al. (1991) interpreted the (core-rim) zoned spinels that they observed as relict grains in which the Cr-poor cores survived melting of the host inclusion, and relatively Cr-rich spinel enclosed them during subsequent crystallization. Another way to derive core-rim spinel grains from a liquid, as shown by FISK and BENCE (1980), is for plagioclase to begin to cocrystallize with spinel. This increases the Cr/Al ratio of the residual liquid and of the crystallizing spinel, but this sequence would only give rise to zoned spinels with corroded cores if, prior to plagioclase crystallization, the liquid composition had left the spinel stability field, causing the spinel to begin to react with the liquid.

Among the separated spinels, we found only two which fall into this group. In one of these, SP5, the core and rim differ sharply not only in Cr_2O_3, TiO_2, and V_2O_3 contents but also in their TiO_2/V_2O_3 ratios (Fig. 7c). This feature, along with the corroded core (Fig. 1h), requires at least a two-stage history: formation of the Cr-poor core, followed by reaction with the surrounding medium and deposition from it of the Cr-rich layers.

Chevron-type grains

Among the separated spinels, three grains of this type (SP44, SP50, and SP76) have only two or three zones, like olivine crystals in some chondrules in Semarkona (JONES, 1990). The remaining chevron-type grains and SP5, with their multiple layers of varying Cr_2O_3 contents, may be analogous to orthopyroxenes with oscillatory FeO zoning found in a Semarkona chondrule by JONES (1993). Because it is unlikely that a molten chondrule would experience repeated additions of material, or repeated changes in physicochemical conditions while still molten, the oscillatory zoning probably reflects formation of boundary layers which were alternately enriched and depleted in FeO because crystal growth was faster than diffusion (e.g., SIBLEY et al., 1976). The chevron-zoned spinel grains discussed here could have formed this way, although no observations of such spinel grains have ever been reported from chondrules.

Gas-solid condensation is also a possible origin for the chevron-zoned grains, because a crystal could easily be exposed to multiple changes in temperature and oxygen fugacity in a nebular environment. This mode of origin is not straightforward, however, for several reasons. During equilibrium condensation from a gas of solar composition, the first spinel to condense should do so prior to forsterite and should be pure $MgAl_2O_4$ (GROSSMAN, 1972). At equilibrium, this spinel reacts with the gas, gradually increasing its Cr content with falling temperature. This process should cause Cr to increase gradually from core to rim, and such a trend is not observed in the concentrically zoned grains considered here.

In addition, new calculations show that this method would not yield spinel with the high Cr and Fe contents that are

characteristic of the separated spinel grains. The same computer program used by LATTIMER and GROSSMAN (1978) was employed in this work to calculate the relative proportions and compositions of minerals that would condense at complete chemical equilibrium from a cooling gas of solar composition. For these calculations, the thermodynamic data used by LATTIMER and GROSSMAN (1978) were updated with free energy data for most silicate and oxide phases from ROBIE et al. (1978), anorthite and gehlenite from ROBINSON et al. (1982), and hibonite and $CaAl_4O_7$ from GEIGER et al. (1988). For diopside and akermanite, the data of ROBIE et al. (1978) were corrected for revised enthalpies of formation from CHARLU et al. (1978) and CHARLU et al. (1981), respectively. Free energy data for $MgAl_2O_4$ are taken from CHAMBERLIN et al. (1991 and pers. commun.). Lack of thermodynamic data for $FeAl_2O_4$ and $FeCr_2O_4$ prevented LATTIMER and GROSSMAN (1978) from investigating the composition of condensate spinel. For $MgCr_2O_4$, $FeCr_2O_4$, and $FeAl_2O_4$, the work of SACK and GHIORSO (1991) was used for the enthalpy and entropy of formation from the elements at 298 K and for the heat capacity versus temperature function. Ideal solution was assumed for the spinel. According to R. O. Sack (pers. commun.), this is an excellent assumption for all spinel compositions encountered in this work. When it is assumed that the identity of the divalent ion entering the spinel structure is independent of the identity of the trivalent ion, thermodynamic data are required for only three of the four spinel components discussed here in order to specify the spinel composition completely. Measurement errors in the free energies of each of the spinel endmember components lead, however, to inconsistencies between them, such that the spinel composition predicted here at a given pressure and temperature depends on which three of the four components are used in the computations.

Results of these calculations are very similar to those of LATTIMER and GROSSMAN (1978), except that the appearance of spinel in the condensation sequence at a total pressure of 10^{-3} atm is delayed by ~55°, until 1476 K where spinel forms by complete reaction of hibonite with the gas and joins the pre-existing condensates, perovskite and melilite. Depending on which spinel components are used, the atomic Cr/(Cr + Al) ratio of the spinel is $1.6 - 3.5 \times 10^{-3}$ at 1470 K and gradually increases to $1.2\text{–}2.6 \times 10^{-2}$ at 1415 K, the temperature at which spinel disappears by reaction with the gas to form anorthite. Over this temperature interval, the atomic Fe/(Fe + Mg) ratio gradually falls from $1.0\text{–}4.9 \times 10^{-3}$ to $4.5 \times 10^{-4}\text{–}2.1 \times 10^{-3}$. At 10^{-4} atm total pressure, the maximum Cr/(Cr + Al) is 2.8×10^{-2} and the maximum Fe/(Fe + Mg) is 1×10^{-3}. According to these calculations, spinel grains that condensed at equilibrium from a gas of solar composition should contain no less than 97 mol% $MgAl_2O_4$, with no more than 3.0 wt% Cr_2O_3 and 0.30 wt% FeO. Regardless of their zoning patterns, the vast majority of the spinel grains described in this paper could not have formed in this way.

Perhaps condensation of spinel was metastably delayed or continued until Cr-rich spinel could condense, and the olivine acted as a nucleus for crystallization. Our calculations suggest that if spinel were to continue to condense, rather than react with the gas to form anorthite, the Cr content of spinel would continue to increase. The high Fe contents in spinel would remain a problem, however, because a solar gas is sufficiently reducing that very little FeO is expected at these high temperatures.

Patchy grains

Exsolution is an unlikely explanation for the patchy zoning patterns reported here, although the textures are similar to those described by MUIR and NALDRETT (1973) and attributed by them to exsolution. Those samples, however, contain very wide ranges of Al_2O_3 (4–40 wt%) and Fe_2O_3 (e.g., 7–50 wt%), and the existence of a large miscibility gap below 900°C for spinels of such compositions has been known for some time (e.g., TURNOCK and EUGSTER, 1962; LEHMANN and ROUX, 1986). These gaps are also predicted from thermodynamic data (LEHMANN and ROUX, 1986; SACK and GHIORSO, 1991). For the compositions observed in the patchy Murchison spinels, no miscibility gaps have been observed experimentally and only very small gaps are predicted between Mg-, Al-rich and Fe-, Cr-rich spinel, but at temperatures below ~500°C. Application of the olivine-spinel geothermometer (ENGI, 1983) to our samples (where possible), gives temperatures of 600°C or more in all cases. Furthermore, comparison of the data for patchy spinels with the calculated curves of SACK and GHIORSO (1991) shows that, with a maximum Cr# of 0.30 and a minimum Mg# of 0.68, all analyses of the patchy spinels plot on the Mg-rich, Al-rich sides of the calculated miscibility gaps, not on opposite sides, as would be the case if the patches formed by exsolution of immiscible components.

Because spinels with compositions within the above ranges are miscible, the patchy textures cannot be primary equilibrium textures, because the two different compositions of spinel cannot crystallize from the same liquid or gas. Plagioclase with patchy zoning has been observed in terrestrial igneous rocks (VANCE, 1965; ANDERSON, 1984). The patches are more sodic (i.e., more fractionated) than, and have sharp boundaries with, the host crystals, and in some cases individual patches are concentrically zoned (VANCE, 1965). These patchy feldspars probably formed by igneous crystallization followed by partial resorption, and then deposition of relatively fractionated feldspar in the cavities created by resorption (VANCE, 1965; ANDERSON, 1984). This model does not work for the patchy Murchison spinels, however. Some grains have Cr-poor patches and others have Cr-rich ones, so the patches and hosts do not have a consistent composition relationship, as in the patchy feldspars described above. HUTCHEON et al. (1978) reported patchy zoning of Na and Mg in anorthite in several Allende CAIs, which may be the result of metasomatism (I. D. Hutcheon, pers. commun.). If correct, metasomatism would be a possible explanation for the patchy zoning in spinel, but no convincing models have been presented.

Because it therefore seems unlikely that the patchy spinel grains were ever molten, we conclude that these grains most likely formed by sintering of aggregates of smaller, probably condensate, spinel grains which were enriched in Cr and probably Fe to varying degrees. Although most contacts between Cr-rich and Cr-poor patches are blurred, the hetero-

geneities in Cr (and Al) have been largely preserved while those in Fe (and Mg) have been mostly erased by diffusion during heating (see, e.g., Fig. 5). Although not proven experimentally, there have been previous suggestions that Cr-Al diffusion is slower than that of Mg and Fe in Cr-spinel. FUDALI and NOONAN (1975) suggested this based on much wider ranges in Cr/Al ratios than in Mg/Fe ratios in spinels in Gobabeb and Mezö-Madaras. MCCOY et al. (1991) found this consistent with their observations as well. They concluded that the Al-Cr zoning in the spinels they analyzed was primary, whereas the Fe-Mg-Zn zoning could have been altered during metamorphism.

The sintering model can explain several features of the patchy spinel grains. Derivation of the patches from individual grains with square-to-rectangular cross-sections and different compositions would explain why some grains, such as SP60 (Fig. 1b), have square- to rectangular-shaped patches. In some cases, as in SP4, 7-20, and M1, coarse olivine was present at the time of heating, and it became rounded, with spinel tending to enclose it. The concave indentations in the spinel give it an elongated, scalloped outline against adjacent silicates, reminiscent of "holly-leaf"-shaped spinels, which are observed in some partially recrystallized ultramafic xenoliths and are thought to form by clumping of smaller, interstitial spinels during recrystallization (e.g., PIKE and SCHWARZMAN, 1977). Compare, for example, the rounded olivine partially enclosed by spinel in M1 (Fig. 2a), 4377-1 (Fig. 2b), and 7-20 (Fig. 2c,d) with the angular, subhedral olivine partially enclosed by spinel in chondrules with probable primary textures (Fig. 11a,b) and in SP73 (Fig. 11c). Exsolution of high- and low-Ca pyroxene from each other and of Fe from olivine in 4377-1 are also indicative of re-equilibration in that inclusion. Thus, recrystallization of an olivine-bearing assemblage is consistent with the observed textures and does not require formation of olivine before spinel. In two places where patchy spinel is in contact with the meteorite matrix (Fig. 2a,c), there is no relationship between the distribution of the patches and the matrix, indicating that the patchiness formed prior to accretion of Murchison, which is also consistent with this model.

Patchy spinel grains may be the end products of sintering of spinel-rich aggregates which originally consisted of many small grains with different compositions. We found several, unsintered, apparently loosely packed, spinel-rich aggregates in Murchison, including one (Fig. 13a) that is $\sim 130 \times 100$ μm and consists of $\sim$90% spinel and $\sim$10% olivine, with minor amounts of aluminous diopside. Most of the spinel and olivine grains are 5–10 μm across. As shown in Fig. 13b, some of the spinel grains in the inclusion, like those in the separates, have round cavities and, like the one at the bottom of Fig. 13b, inclusions of Ca-silicate (too small to analyze in this case). There are gaps between most of the grains but, at the center of Fig. 13b, there are several grains connected to others. Individual spinel grains are homogeneous but, for the whole inclusion, Cr_2O_3 contents in the spinel grains range from 1.0 to 1.6 wt%, FeO ranges from 0.8 to 7.9 wt%, and the olivine composition is Fo_{90}-Fo_{95}. It seems reasonable to suggest that, if such an aggregate were heated sufficiently, the individual grains would grow together into a single, heterogeneous one with some of the gaps between precursor grains and some of the holes in them partially to completely filled with aluminous diopside or other material. Samples SP58 (Fig. 13c) and SP60 (Fig. 1b) may represent an intermediate step in the sequence from a loose aggregate (Fig. 13a,b) to a patchy grain with some gaps and former grain boundaries to a less porous patchy grain, e.g., SP51 (Fig. 1c) and SP64 (Fig. 1d).

Electron probe data show that the patches do not appear to represent two distinct populations of precursor grains. The high-Cr and low-Cr patches vary in composition from grain to grain (Table 1) and, within individual grains, composition gaps are small to nonexistent whether the contacts between the grains are sharp or diffuse (Fig. 5). Their minor element contents may overlap (Fig. 5b), or they may be suggestive of mixing between Cr-, Ti-, V-rich and Cr-, Ti-, V-poor spinel (Fig. 5d). Patches probably represent a wide variety of precursor grains that have been modified to varying degrees by diffusion.

Thermal Histories

The presence of zoned and unzoned spinels in Murchison suggests that either heating occurred prior to accretion of the meteorite or unzoned grains were never zoned. The zoned grains that are the most likely to have been modified the least are SP27 (gradational) and SP49 (chevron). Their zoning is probably primary because they are the grains with the strongest zoning in Mg and Fe, which is relatively easily erased by heating. FeO is expected to increase from core to rim in spinel, either due to increased concentration in a residual liquid, as seen in spinel in some chondrules, or to increased availability via condensation from a cooling gas. Cr_2O_3 should increase in spinel during condensation from a solar gas, but can either increase or decrease during crystallization from a liquid, depending upon the liquid composition and the bulk crystal/liquid distribution coefficient of the crystallizing assemblage. In both unequilibrated spinels, Fe and Cr are positively correlated.

Among the patchy spinels, the fact that most have patches with diffuse boundaries, some have sharp boundaries, and a few, e.g., SP41, have both, suggests that these grains have experienced a variety of thermal histories. Presumably those with diffuse boundaries were exposed to higher temperatures and/or heated longer than those with sharp boundaries. In those with both types of contacts, the sharp patches may have formed by mild heating following addition of more spinel grains to an earlier-formed aggregate. The effects of diffusion can be seen in the data for SP51 (Fig. 5c,d). The Fe/Mg ratios of the patches are uniform but the minor element zoning is preserved. Unfortunately, not enough is known about diffusion rates in spinels of these compositions to allow us to estimate temperatures or cooling rates.

It is unlikely that spinel would be melted upon reheating because of its high melting point, but included silicate might and, if cooled quickly enough, could give rise to the glass inclusions observed in several patchy grains. These glasses are SiO_2-, CaO-, and Al_2O_3-rich and MgO-poor (Table 5). Liquids with these compositions would be in equilibrium with anorthite, not spinel. They probably do not represent trapped parental melts, but could be quenched melts of silicate inclusions that were present at the time of heating.

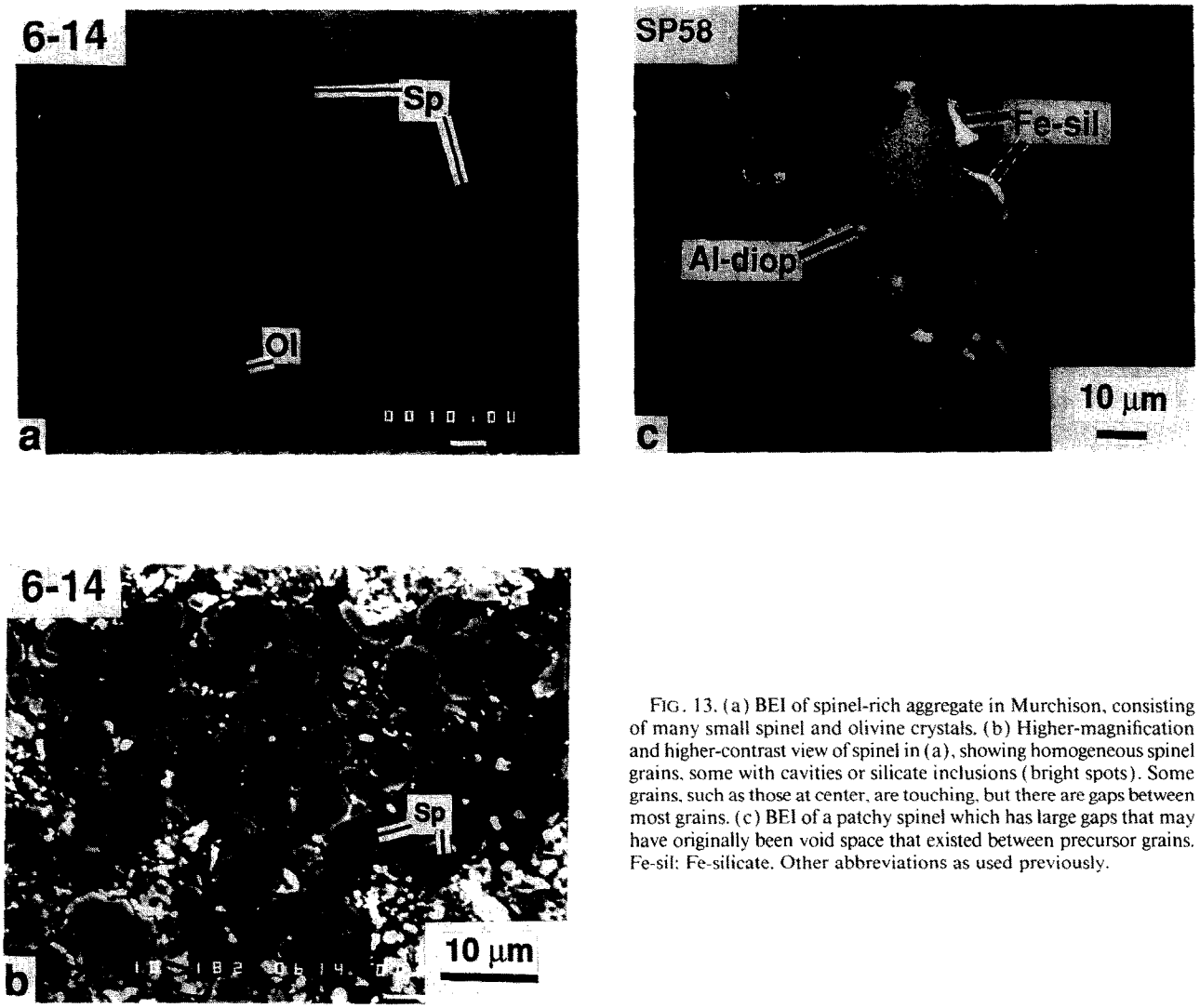

FIG. 13. (a) BEI of spinel-rich aggregate in Murchison, consisting of many small spinel and olivine crystals. (b) Higher-magnification and higher-contrast view of spinel in (a), showing homogeneous spinel grains, some with cavities or silicate inclusions (bright spots). Some grains, such as those at center, are touching, but there are gaps between most grains. (c) BEI of a patchy spinel which has large gaps that may have originally been void space that existed between precursor grains. Fe-sil: Fe-silicate. Other abbreviations as used previously.

Isotopic Histories

According to their oxygen isotopic compositions, there exist at least two types of spinel in Murchison. The oxygen isotopic composition of the Cr-rich spinel grains of this study is close to normal with an average composition of $\delta^{17}O = -0.9 \pm 1.4‰$ and $\delta^{18}O = 1.9 \pm 2.4‰$. In contrast, the average oxygen isotopic composition of nine pure Mg-, Al-spinel grains from Murchison acid residue CFOc is $\delta^{17}O = -49.4 \pm 1.5‰$ and $\delta^{18}O = -49.9 \pm 3.1‰$ (VIRAG et al., 1991). The latter spinels probably originate in refractory inclusions, as IRELAND et al. (1992) found oxygen isotopic compositions comparable to theirs in spinels from spinel-hibonite and spinel-perovskite inclusions from Murchison.

The composition of the spinel-rich residue 2C10c ($\delta^{17}O = -41.1‰$; $\delta^{18}O = -39.8‰$) measured by CLAYTON and MAYEDA (1984) would thus represent a mixture of these two components. If we assume that only these two classes of spinel contribute to the oxygen analyzed by CLAYTON and MAYEDA (1984), we calculate a ratio of ^{16}O-rich, Mg-, Al-spinel to isotopically normal, Cr-rich spinel of 4.6 ± 0.7. This ratio would decrease if hibonite and corundum grains, which are at least as ^{16}O-rich as the Mg-, Al-spinels (FAHEY et al., 1987; VIRAG et al., 1991; IRELAND et al., 1992) and are known to exist in the residues, are taken into consideration. On the other hand, residue 2C10c may also contain other phases with oxygen that is less ^{16}O-rich than the average measured by CLAYTON and MAYEDA (1984). Fe-chromite and Fe-oxide grains have been seen in CFOc (ZINNER and EPSTEIN, 1987; VIRAG et al., 1991) but their abundances in the residue are not known.

A fundamental question is whether or not the oxygen isotopic composition of the Cr-bearing spinel grains of the present study can provide any information regarding the time of their formation. In order to explain the isotopic variations among different mineral phases from Allende Ca-, Al-rich inclusions, CLAYTON et al. (1977) proposed the diffusion exchange model. According to this model, these inclusions were formed with ^{16}O enrichments of approximately 5% but subsequently some phases, such as melilite, equilibrated with a gas reservoir containing isotopically normal oxygen while spinel retained its original oxygen isotopic composition. Unfortunately, the conclusions that can be drawn from the essentially normal oxygen isotopic composition of the Cr-bear-

ing spinel grains are limited by the lack of knowledge of their thermal history and of the oxygen diffusion rate in spinel as a function of Fe and Cr content. If the time-temperature history of the spinels was similar to those of Allende CAIs it does not seem reasonable to propose that the relatively large ($\sim$100 μm), patchy spinel grains studied here were able to exchange their oxygen completely, converting original ^{16}O-rich compositions to normal oxygen isotopic compositions, while the much smaller ($\sim$30 μm) spinel grains in the Allende refractory inclusions were unable to do so. However, large Murchison spinels *could* have cooled much more slowly than Allende CAIs. The model suggested above, for the origin of patchy spinels, envisions their formation by sintering of a pre-existing generation of spinel grains which may have been approximately the same size as those in the Allende inclusions. If the precursor grains were originally ^{16}O-rich, their higher Cr contents could have led to significantly enhanced rates of oxygen diffusion compared to spinel in Allende inclusions, allowing them to exchange with a reservoir of normal oxygen isotopic composition. Although diffusion in chromite spinels is generally faster than in aluminate spinels (BIRCHENALL, 1968), we do not know whether the substitution of Fe for Mg and Cr for Al in Mg-, Al-spinel to the extent observed here has any effect on the diffusion coefficient of oxygen. We note that, while SP36 is among the spinel grains with normal oxygen isotopic composition, it has only 1.5–2.0% Cr_2O_3 and 0.5% FeO (Table 1).

At this point we cannot determine whether the precursor grains formed initially in a reservoir with isotopically normal oxygen or whether the spinel grains exchanged their originally ^{16}O-rich oxygen either because they experienced slow cooling or because the oxygen diffusion in Cr-bearing spinel is significantly faster than in pure Mg-, Al-spinel.

A more promising approach is to compare oxygen diffusion with cation diffusion rates. Generally, cation diffusion in oxides is faster than diffusion of oxygen. For example, Al diffuses faster than O in Al_2O_3 (PALADINO and KINGERY, 1962; REDDY and COOPER, 1982) and in MgO (LINDNER and PARFITT, 1957; REDDY and COOPER, 1983). This is in marked contrast to gehlenite, where oxygen diffusion is faster than cation diffusion (MORIOKA et al., 1987), consistent with the CLAYTON et al. (1977) oxygen exchange model for chemically zoned melilite in Allende CAIs. If Al and Cr diffuse faster than oxygen also in Cr-bearing spinels, the obvious lack of extensive Al-Cr interdiffusion in the patchy spinel grains would indicate that their oxygen isotopic compositions did not change since their chemical heterogeneities were established. The argument is even stronger if we consider the diffusion of Fe and Mg. One patchy spinel analyzed for oxygen isotopes (SP31) shows a large range in FeO (Table 1). In pure Mg-, Al-spinel, the self-diffusion coefficient of O is 6.4×10^{-15} cm^{2}s^{-1} at 1553°C (REDDY and COOPER, 1981; RYERSON and MCKEEGAN, 1993), much lower than that of Mg, 8.6×10^{-10} cm^{2}s^{-1}, at the same temperature (SHENG et al., 1992). It is likely that oxygen in these spinel crystals has not re-equilibrated since their Fe-Mg distributions were established. While we can tentatively use these relative diffusion rate considerations to rule out oxygen isotopic exchange of these spinel grains after they became chemically heterogeneous, we cannot rule out the possibility that precursor materials condensed from an ^{16}O-rich reservoir and then exchanged their oxygen with an isotopically normal reservoir prior to the formation of the observed spinel grains.

The chromium isotopic data support formation of homogeneous, gradational, core-rim and patchy spinel from an isotopically normal reservoir within less than one ‰. This conclusion is quite different from that reached by ESAT and IRELAND (1989) who concluded that chromium in their samples was variably anomalous to a greater extent than observed in any other samples, even FUN (mass Fractionation with UNknown nuclear components) inclusions (Fig. 10b). Anomalies of this magnitude are clearly not present in our data, so our results do not support those of ESAT and IRELAND (1989), even though, on the basis of sample preparation technique, size, color, and mineral chemistry, the spinels studied by ESAT and IRELAND (1989) appear to represent a population indistinguishable from that studied here. It should be noted that the absence of chromium anomalies in our data is compatible with the lack of oxygen isotopic anomalies in these spinels (Fig. 9).

A more subtle question is whether the spinels studied here have chromium isotopic anomalies comparable to those endemic in CAI-hosted spinels (PAPANASTASSIOU, 1986; BIRCK and ALLÈGRE, 1988), indicated by the box in Fig. 10a. Because of the larger errors involved in single-grain measurements, it is difficult to address the question on a grain-by-grain basis. Taken in aggregate, our data suggest that the large chromian spinels do not have the endemic chromium anomalies of CAI spinels but, in view of the analytical errors, this is only a suggestion which deserves further study. The endemic ^{54}Cr excess is generally regarded as a nucleosynthetic anomaly, i.e., as a manifestation that these samples formed from a reservoir in which different types of presolar materials, bearing different nucleosynthetic products, were not well mixed. In view of the oxygen isotopic evidence that the chromian spinels could have formed from a more nearly normal (well-mixed) reservoir than spinels from CAIs, absence of ^{54}Cr anomalies is not surprising.

The endemic deficit of ^{53}Cr in spinels from CAIs, however, is not generally considered to be a nucleosynthetic anomaly, but a "ghost" of ^{53}Mn; some 1–2 ϵ of present normal ^{53}Cr was evidently formed by decay of ^{53}Mn (half-life = 3.7 Ma) which was extant in the early solar system, and early formed materials with low Mn/Cr ratios, such as meteoritic spinel, should lack this much ^{53}Cr.

SUMMARY AND CONCLUSIONS

Unlike the spinels from refractory inclusions, those studied here are coarse and contain weight percent levels of FeO and Cr_2O_3, but have higher Mg/Fe and Al/Cr ratios than spinel (chromites) from ferromagnesian chondrules. Five zoning types (with respect to their Cr/Al ratios) are recognized: patchy, homogeneous, gradational, chevron, and core-rim. Many have inclusions of aluminous diopside and/or partially enclose forsteritic olivine. Neither the high Cr and Fe contents of the spinels nor the crystallization sequence of spinel after olivine indicated by the textures, if they are primary, are consistent with equilibrium condensation from a gas of solar composition. This sequence is observed, however, in some

Al-rich chondrules in Murchison, and such chondrules may have been the sources of some of the spinel grains described here. Homogeneous, gradational-zoned, and core-rim spinels have been found in such chondrules, demonstrating that these types of grains can crystallize from liquids. The chevron-zoned grains could have formed in chondrules, although no such spinels have ever been reported in a chondrule. An origin by gas-solid condensation is also possible for these grains, but a gas more oxidizing than a solar gas would be required. Patchy spinel grains probably formed from spinel-rich aggregates by solid-state recrystallization during heating, which caused pre-existing spinel grains to grow together and homogenized Mg/Fe ratios but caused only minor interdiffusion of Cr and Al. The spinel grains are isotopically uniform and lack the oxygen and possibly the chromium isotopic anomalies observed in spinels from CAIs, indicating formation from a normal, well-mixed reservoir.

Acknowledgments—We thank the following for loans of Murchison thin sections: A. Brearly (University of New Mexico); I. Casanova (Field Museum of Natural History); M. Prinz (American Museum of Natural History); and I. Steele (University of Chicago). Discussions with J. Beckett and I. Casanova were helpful, as were reviews by A. El Goresy, I. Hutcheon, and G. Lugmair. J. Lattimer performed condensation calculations, S. Yoneda assisted with Fig. 10, and A. Davis with Fig. 12b. This work was supported by NASA grants NAG 9-54 (LG), NAGW-3340 (LG), NAG 9-55 (EZ), and NAG 9-292 (FAP).

REFERENCES

ANDERSON A. T., JR. (1984) Probable relations between plagioclase zoning and magma dynamics, Fuego Volcano, Guatemala. *Amer. Mineral.* **69**, 660–676.

BIRCHENALL C. E. (1968) Diffusion in oxides: Assessment of existing data and experimental problems. In *Mass Transport in Oxides* (ed. J. B. WACHTMAN JR. and A. D. FRANKLIN); *National Bureau of Standards Special Publication 296*, pp. 119–127.

BIRCK J.-L. and ALLÈGRE C. J. (1988) Manganese-chromium isotope systematics and development of the early solar system. *Nature* **331**, 579–584.

BISCHOFF A. and KEIL K. (1983) Catalog of Al-rich chondrules, inclusions and fragments in ordinary chondrites. *Spec. Pub. 22.* Univ. New Mexico Institute of Meteoritics.

BISCHOFF A. and KEIL K. (1984) Al-rich objects in ordinary chondrites: Related origin of carbonaceous and ordinary chondrites and their constituents. *Geochim. Cosmochim. Acta* **48**, 693–709.

CHAMBERLIN L., BECKETT J. R., and STOLPER E. M. (1991) Experimental determination of the free energy of formation of $MgAl_2O_4$ spinel: An important constraint on solar system processes. *Lunar Planet. Sci. XXII*, 195–196 (abstr.).

CHARLU T. V., NEWTON R. C., and KLEPPA O. J. (1978) Enthalpy of formation of some lime silicates by high-temperature solution calorimetry, with discussion of high pressure phase equilibria. *Geochim. Cosmochim. Acta* **42**, 367–375.

CHARLU T. V., NEWTON R. C., and KLEPPA O. J. (1981) Thermochemistry of synthetic $Ca_2Al_2SiO_7$ (gehlenite)-$Ca_2MgSi_2O_7$ (åkermanite) melilite. *Geochim. Cosmochim. Acta* **45**, 1609–1617.

CLAYTON R. N. and MAYEDA T. K. (1984) The oxygen isotope record in Murchison and other carbonaceous chondrites. *Earth Planet. Sci. Lett.* **67**, 151–161.

CLAYTON R. N., ONUMA N., GROSSMAN L., and MAYEDA T. K. (1977) Distribution of the pre-solar component in Allende and other carbonaceous chondrites. *Earth Planet. Sci. Lett.* **34**, 209–224.

EL GORESY A., RAMDOHR P., and TAYLOR L. A. (1971) The opaque minerals in the lunar rocks from Oceanus Procellarum. *Proc. 2nd Lunar Sci. Conf.*, 219–235.

EL GORESY A., PRINZ M., and RAMDOHR P. (1976) Zoning in spinels as an indicator of the crystallization histories of mare basalts. *Proc. 7th Lunar Sci. Conf.*, 1261–1279.

ENGI M. (1983) Equilibria involving Al-Cr spinel: Mg-Fe exchange with olivine. Experiments, thermodynamic analysis and consequences for geothermometry. *Amer. J. Sci.* **283A**, 29–71.

ESAT T. M. and IRELAND T. R. (1989) Chromium isotopic anomalies in the Murchison meteorite. *Earth Planet. Sci. Lett.* **92**, 1–6.

FAHEY A. J., GOSWAMI J. N., MCKEEGAN K. D., and ZINNER E. (1987) ^{16}O excesses in Murchison and Murray hibonites: A case against a late supernova injection origin of isotopic anomalies in O, Mg, Ca and Ti. *Ap. J.* (Lett.) **323**, L91–L95.

FISK M. R. and BENCE A. E. (1980) Experimental crystallization of chrome spinel in FAMOUS basalt 527-1-1. *Earth Planet. Sci. Lett.* **48**, 111–123.

FUCHS L. H., OLSEN E., and JENSEN K. J. (1973) Mineralogy, mineral-chemistry and composition of the Murchison (C2) meteorite. *Smithsonian Contrib. Earth Sci.* **10**.

FUDALI R. F. and NOONAN A. F. (1975) Gobabeb, a new chondrite: The coexistence of equilibrated silicates and unequilibrated spinels. *Meteoritics* **10**, 31–39.

GEIGER C. A., KLEPPA O. J., MYSEN B. O., LATTIMER J. M., and GROSSMAN L. (1988) Enthalpies of formation of $CaAl_4O_7$ and $CaAl_{12}O_{19}$ (hibonite) by high temperature, alkali borate calorimetry. *Geochim. Cosmochim. Acta* **52**, 1729–1736.

GROSSMAN L. (1972) Condensation, chondrites and planets. Ph.D. dissertation, Yale Univ.

GROSSMAN L., FAHEY A. J., and ZINNER E. (1988) Carbon and oxygen isotopic compositions of individual spinel crystals from the Murchison meteorite. *Lunar Planet. Sci. XIX*, 435–436 (abstr.).

HAGGERTY S. E. (1972) Luna 16: An opaque mineral study and a systematic examination of compositional variations of spinels from Mare Fecunditatis. *Earth Planet. Sci. Lett.* **13**, 328–352.

HUTCHEON I. D., STEELE I. M., SMITH J. V., and CLAYTON R. N. (1978) Ion microprobe, electron microprobe and cathodoluminescence data for Allende inclusions with emphasis on plagioclase chemistry. *Proc. 9th Lunar Planet. Sci. Conf.*, 1345–1368.

IRELAND T. R., ZINNER E. K., FAHEY A. J., and ESAT T. M. (1992) Evidence for distillation in the formation of HAL and related hibonite inclusions. *Geochim. Cosmochim. Acta* **56**, 2503–2520.

IRVING A. J. (1978) A review of experimental studies of crystal/liquid trace element partitioning. *Geochim. Cosmochim. Acta* **42**, 743–770.

JOHNSON C. A. and PRINZ M. (1991) Chromite and olivine in type II chondrules in carbonaceous and ordinary chondrites: Implications for thermal histories and group differences. *Geochim. Cosmochim. Acta* **55**, 893–904.

JONES R. H. (1990) Petrology and mineralogy of Type II, FeO-rich chondrules in Semarkona (LL3.0): Origin by closed-system fractional crystallization, with evidence for supercooling. *Geochim. Cosmochim. Acta* **54**, 1785–1802.

JONES R. H. (1992) On the relationship between isolated and chondrule olivine grains in the carbonaceous chondrite ALHA77307. *Geochim. Cosmochim. Acta* **56**, 467–482.

JONES R. H. (1993) Complex zoning behavior in pyroxene in FeO-rich chondrules in the Semarkona ordinary chondrite. *Lunar Planet. Sci. XXIV*, 735–736 (abstr.).

JONES R. H. and SCOTT E. R. D. (1989) Petrology and thermal history of type IA chondrules in the Semarkona (LL3.0) chondrite. *Proc. 19th Lunar Planet. Sci. Conf.*, 523–536.

KUEHNER S. M. and GROSSMAN L. (1987) Petrography and mineral chemistry of spinel grains separated from the Murchison meteorite. *Lunar Planet. Sci. XVIII*, 519–520 (abstr.).

LATTIMER J. M. and GROSSMAN L. (1978) Chemical condensation sequences in supernova ejecta. *Moon and Planets* **19**, 169–184.

LEHMANN J. and ROUX J. (1986) Experimental and theoretical study of $(Fe^{2+}, Mg)(Al, Fe^{3+})_2O_4$ spinels: Activity-composition relationships, miscibility gaps, vacancy contents. *Geochim. Cosmochim. Acta* **50**, 1765–1783.

LINDNER R. and PARFITT G. D. (1957) Diffusion of radioactive magnesium in magnesium oxide crystals. *J. Chem. Phys.* **26**, 182–185.

MACPHERSON G. J., BAR-MATTHEWS M., TANAKA T., OLSEN E., and GROSSMAN L. (1980) Refractory inclusions in Murchison:

Recovery and mineralogical description. *Lunar Planet. Sci. XI*. 660–662 (abstr.).

MACPHERSON G. J., BAR-MATTHEWS M., TANAKA T., OLSEN E., and GROSSMAN L. (1983) Refractory inclusions in the Murchison meteorite. *Geochim. Cosmochim. Acta* **47**, 823–839.

MACPHERSON G. J., GROSSMAN L., HASHIMOTO A., BAR-MATTHEWS M., and TANAKA T. (1984a) Petrographic studies of refractory inclusions from the Murchison meteorite. *Proc. 15th Lunar Planet. Sci. Conf.: J. Geophys. Res.* **89** (supplement), C299–C312.

MACPHERSON G. J., PAQUE J. M., STOLPER E., and GROSSMAN L. (1984b) The origin and significance of reverse zoning in melilite from Allende Type B inclusions. *J. Geol.* **92**, 289–305.

MCCOY T. J., PUN A., and KEIL K. (1991) Spinel-bearing, Al-rich chondrules in two chondrite finds from Roosevelt County, New Mexico: Indicators of nebular and parent body processes. *Meteoritics* **26**, 301–309.

MCKEEGAN K. D. (1987) Oxygen isotopes in refractory stratospheric dust particles: Proof of extraterrestrial origin. *Science* **237**, 1468–1471.

MIYAMOTO M., FURUTA T., FUJII N., MCKAY D. S., LOFGREN G. E., and DUKE M. B. (1993) The Mn-Fe negative correlation in olivines in ALHA77257 ureilite. *J. Geophys. Res.* **98**, 5301–5307.

MORIOKA M., YURIMOTO H., IGUSA T., and NAGASAWA H. (1987) Diffusion coefficients of cations and oxygen in synthesized single crystal melilites and their implications to the thermal history of Allende CAI. *Lunar Planet. Sci. XVIII*, 665–666 (abstr.).

MUIR J. E. and NALDRETT A. J. (1973) A natural occurrence of two-phase chromium-bearing spinels. *Canadian Mineral.* **11**, 930–939.

NEUVONEN K. J., OHLSON B., PAPUNEN H., HÄKLI T. A., and RAMDOHR P. (1972) The Haverö ureilite. *Meteoritics* **7**, 515–531.

OLSEN E. and GROSSMAN L. (1978) On the origin of isolated olivine grains in Type 2 carbonaceous chondrites. *Earth Planet. Sci. Lett.* **41**, 111–127.

OSBORN E. F., DEVRIES R. C., GEE K. H., and KRANER H. M. (1954) Optimum composition of blast-furnace slags as deduced from liquidus data for the quaternary system CaO-MgO-Al_2O_3-SiO_2. *Trans. AIME* **200**, 33–45.

OSBORN T. W., WARREN R. G., SMITH R. H., WAKITA H., ZELLMER D. L., and SCHMITT R. A. (1974) Elemental composition of individual chondrules from carbonaceous chondrites, including Allende. *Geochim. Cosmochim. Acta* **38**, 1359–1378.

PALADINO A. E. and KINGERY W. D. (1962) Aluminum ion diffusion in aluminum oxide. *J. Chem. Phys.* **37**, 957–962.

PAPANASTASSIOU D. A. (1986) Chromium isotopic anomalies in the Allende meteorite. *Ap. J.* **308**, L27–L30.

PIKE J. E. N. and SCHWARZMAN E. C. (1977) Classification of textures in ultramafic xenoliths. *J. Geol.* **85**, 49–61.

PODOSEK F. A., PROMBO C. A., GROSSMAN L., and ZINNER E. (1991) Chromium isotopic compositions of individual spinel crystals from the Murchison meteorite. *Meteoritics* **26**, 385–386 (abstr.).

POUCHOU J. L. and PICHOIR F. (1984) A new model for quantitative x-ray microanalysis. Part I: Application to the analysis of homogeneous samples. *Rech. Aerosp.* **1984-3**, 13–38.

REDDY K. P. R. and COOPER A. R. (1981) Oxygen diffusion in magnesium aluminate spinel. *J. Amer. Ceram. Soc.* **64**, 368–371.

REDDY K. P. R. and COOPER A. R. (1982) Oxygen diffusion in sapphire. *J. Amer. Ceram. Soc.* **65**, 634–638.

REDDY K. P. R. and COOPER A. R. (1983) Oxygen diffusion in MgO and α-Fe_2O_3. *J. Amer. Ceram. Soc.* **66**, 664–666.

ROBIE R. A., HEMINGWAY B. S., and FISHER J. R. (1978) Thermodynamic properties of minerals and related substances at 298.15K and 1 Bar (10^5 Pascals) pressure and at higher temperatures. *USGS Bull. 1452*.

ROBINSON G. R., JR., HAAS J. L., JR., SCHAFER C. M., and HASELTON H. T., JR. (1982) Thermodynamic and thermophysical properties of selected phases in the MgO-SiO_2-H_2O-CO_2, CaO-Al_2O_3-SiO_2-H_2O-CO_2, and Fe-FeO-Fe_2O_3-SiO_2 chemical systems, with special emphasis on the properties of basalts and their mineral components. *USGS Open-File Rept. 83-79*.

ROEDDER E. (1981) Significance of Ca-Al silicate melt inclusions in olivine crystals from the Murchison type II carbonaceous chondrite. *Bull. Mineral.* **104**, 339–353.

RUSSELL W. A., PAPANASTASSIOU D. A., and TOMBRELLO T. A. (1978) Calcium isotope fractionation on the Earth and in other solar system materials. *Geochim. Cosmochim. Acta* **42**, 1075–1090.

RYERSON F. J. and MCKEEGAN K. D. (1993) Determination of oxygen self-diffusion in åkermanite, anorthite, diopside and spinel: Implications for oxygen isotopic anomalies and the thermal histories of Ca-Al-rich inclusions. *Geochim. Cosmochim. Acta* (in review).

SACK R. O. and GHIORSO M. S. (1991) Chromian spinels as petrogenetic indicators: Thermodynamics and petrological applications. *Amer. Mineral.* **76**, 827–847.

SHENG Y. J., HUTCHEON I. D., and WASSERBURG G. J. (1991) Origin of plagioclase-olivine inclusions in carbonaceous chondrites. *Geochim. Cosmochim. Acta* **55**, 581–599.

SHENG Y. J., WASSERBURG G. J., and HUTCHEON I. D. (1992) Self-diffusion of magnesium in spinel and equilibrium melts: Constraints on flash heating of silicates. *Geochim. Cosmochim. Acta* **56**, 2535–2546.

SHIELDS W. R., MURPHY T. J., CATANZARO E. J., and CARNER E. L. (1966) Absolute isotope abundance ratios and the atomic weight of a reference sample of chromium. *J. Res. NBS* **70A**, 193–197.

SIBLEY D. F., VOGEL T. A., WALKER B. M., and BYERLY G. (1976) The origin of oscillatory zoning in plagioclase: A diffusion and growth controlled model. *Amer. J. Sci.* **276**, 275–284.

SIMON S. B. and GROSSMAN L. (1992) Petrography, composition and origin of chromian spinel crystals separated from the Murchison meteorite. *Lunar Planet. Sci. XXIII*, 1299–1300 (abstr.).

STEELE I. M. (1990) Minor elements in forsterites of Orgueil (C1), Alais (C1) and two interplanetary dust particles compared to C2-C3-UOC forsterites. *Meteoritics* **25**, 301–307.

STOLPER E. (1982) Crystallization sequences of Ca-Al-rich inclusions from Allende: An experimental study. *Geochim. Cosmochim. Acta* **46**, 2159–2180.

TOMEOKA K. and BUSECK P. R. (1985) Indicators of aqueous alteration in CM carbonaceous chondrites: Microtextures of a layered mineral containing Fe, S, O and Ni. *Geochim. Cosmochim. Acta* **49**, 2149–2163.

TURNOCK A. C. and EUGSTER H. P. (1962) Fe-Al oxides: Phase relationships below 1000°C. *J. Petrol.* **3**, 533–565.

VANCE J. A. (1965) Zoning in igneous plagioclase: Patchy zoning. *J. Geol.* **73**, 636–651.

VIRAG A., ZINNER E., AMARI S., and ANDERS E. (1991) An ion microprobe study of corundum in the Murchison meteorite: Implications for ^{26}Al and ^{16}O in the early solar system. *Geochim. Cosmochim. Acta* **55**, 2045–2062.

YANG H.-Y. (1975) Al- and Ti-rich clinopyroxene in the system $CaMgSi_2O_6$-$CaAl_2SiO_6$-$CaTiAl_2O_6$. *Proc. Geol. Soc. China* **18**, 48–58.

ZINNER E. and EPSTEIN S. (1986) Heavy carbon in individual oxide grains from Murchison acid residue CFOc. *Lunar Planet. Sci. XVII*, 967–968 (abstr.).

ZINNER E. and EPSTEIN S. (1987) Heavy carbon in individual oxide grains from the Murchison meteorite. *Earth Planet. Sci. Lett.* **84**, 359–368.

ZINNER E. K., CAILLET C., and EL GORESY A. (1991) Evidence for extraneous origin of a magnesiowüstite-metal Fremdling from the Vigarano CV3 chondrite. *Earth Planet. Sci. Lett.* **102**, 252–264.